Inorganic Chemistry

Article

pubs.acs.org/IC

Toward Hypoxia-Selective Rhenium and Technetium Tricarbonyl Complexes

Andrea J. North,[†] David J. Hayne,[†] Christine Schieber,[†] Katherine Price,[‡] Anthony R. White,[‡] Peter J. Crouch,[‡] Angela Rigopoulos,[⊥,#,▽] Graeme J. O'Keefe,[§] Henri Tochon-Danguy,[§] Andrew M. Scott,[§,∥,⊥,#] Jonathan M. White,[†] Uwe Ackermann,[§,∥,⊥,#] and Paul S. Donnelly*[,†]

[†]School of Chemistry and Bio21 Molecular Science & Biotechnology Institute, [‡]Department of Pathology, University of Melbourne, Melbourne, Victoria 3010, Australia

[§]Department of Molecular Imaging and Therapy, [∥]Department of Medicine, University of Melbourne, Austin Health, Studley Rd, Heidelberg, Victoria 3010, Australia

[⊥]Olivia Newton-John Cancer Research Institute, [#]School of Cancer Medicine, La Trobe University, Melbourne, Victoria 2086, Australia

[▽]Ludwig Institute for Cancer Research, Melbourne-Austin Branch, 145 Studley Road, Heidelberg, Victoria 3084, Australia

Supporting Information

ABSTRACT: With the aim of preparing hypoxia-selective imaging and therapeutic agents, technetium(I) and rhenium(I) tricarbonyl complexes with pyridylhydrazone, dipyridylamine, and pyridylaminocarboxylate ligands containing nitrobenzyl or nitroimidazole functional groups have been prepared. The rhenium tricarbonyl complexes were synthesized with short reaction times using microwave irradiation. Rhenium tricarbonyl complexes with deprotonated *p*-nitrophenyl pyridylhydrazone ligands are luminescent, and this has been used to track their uptake in HeLa cells using confocal fluorescent microscopy. Selected rhenium tricarbonyl complexes displayed higher uptake in hypoxic cells when compared to normoxic cells. A ^{99m}Tc tricarbonyl complex with a dipyridylamine ligand bearing a nitroimidazole functional group is stable in human serum and was shown to localize in a human renal cell carcinoma (RCC; SK-RC-52) tumor in a mouse.

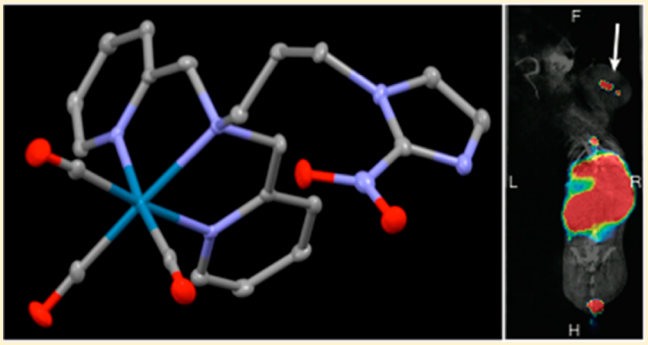

INTRODUCTION

Tissue hypoxia is a complicated condition in which O_2 demand exceeds supply and results in disrupted cellular metabolism. It can occur when vascular dioxygen supply is interrupted after stroke or myocardial infarction, or when a tumor exceeds the vascular diffusion limit for oxygen. Tumors that are hypoxic can be more resistant to traditional therapeutic strategies. Imaging agents that are selectively retained in hypoxic tissue can be detected using noninvasive molecular imaging techniques and have a role to play in increasing the understanding of hypoxia in tumor biology. Hypoxia imaging agents are also useful tools for clinicians when designing and assessing treatment regimes.[1] The molecular imaging technique of positron emission tomography (PET) relies on a positron-emitting molecule, a tracer that is administered to a patient, and the emitted radiation is detected by an external camera. A 2-nitroimidazole, labeled with positron-emitting fluorine-18, ^{18}F-fluoromisonidazole (FMISO; Figure 1a), has been studied as a hypoxia imaging agent.[1−3] It is thought that FMISO is trapped preferentially in hypoxic tissue by virtue of reduction of the nitro functional group, followed by reaction of the reduced hydroxylamine with reactive biomolecules found inside cells. In normal cells, it is argued that any reduced intermediates are rapidly oxidized back to the original nitroimidazole, which is then capable of diffusing back out of the cell. Although FMISO has demonstrated considerable potential as a hypoxia imaging agent, it suffers from relatively slow cell uptake and poor clearance from normoxic tissue.[4−6]

While the number of hospitals equipped with PET infrastructure is increasing, single photon emission computed tomography (SPECT) remains the major technique for nuclear medicine imaging. The most commonly used radioisotope for SPECT is technetium-99m (^{99m}Tc), and unlike ^{18}F that requires a cyclotron for production of tracers, ^{99m}Tc is readily available from commercial generators. The nuclear properties of ^{99m}Tc ($t_{1/2}$ = 6.01 h, E_γ = 141 keV) are ideally suited to diagnostic procedures. A hypoxia-selective ^{99m}Tc radiopharmaceutical that utilizes the more commonly encountered imaging modality of SPECT could be an attractive alternative to ^{18}F

Received: July 26, 2015

DOI: 10.1021/acs.inorgchem.5b01691
Inorg. Chem. XXXX, XXX, XXX−XXX

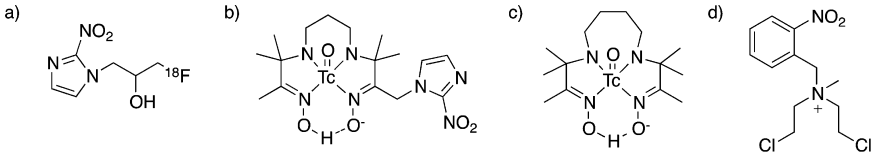

Figure 1. Chemical structures of (a) ^{18}F-FMISO, (b) [TcO(PnAO-1-(2-nitroimidazole)] (BMS 181321), (c) [TcO(BnAO)] (Prognox), and (d) hypoxia-selective nitrobenzyl prodrug, *N,N-bis*(2-chloroethyl)-*N*-methyl-*N*-(2-nitrobenzyl)ammonium chloride.

based 2-nitroimidazole systems. Efforts to produce hypoxia-selective technetium complexes have focused on propylene amine oxime ligands (PnAO) with appended nitroimidazole functional groups such as [TcO(PnAO-1-(2-nitroimidazole)] (Figure 1b). This complex selectively accumulates in hypoxic cells *in vitro*; however its use *in vivo* is limited by high blood uptake and extensive hepatobiliary excretion.[7−9] The $\{Tc^{V}O\}^{3+}$ complex of a butylene amine oxime ligand, [TcO(BnAO)] (also referred to as [TcO(HL91)] or Prognox; Figure 1c), does not contain a nitro functional group but does display some degree of hypoxia selectivity, although the origins of this specificity remain uncertain.[10−12] Peptide-based ligands containing a 2-nitroimidazole functional group for the $\{Tc^{V}O\}^{3+}$ fragment have also been investigated.[13,14]

Bioreductive prodrugs that can undergo enzymatic reduction are generally classified within one of five categories: the nitroaromatics, quinones, aromatic/aliphatic *N*-oxides, or metal complexes.[15] Similarly to 2-nitroimidazoles, nitrobenzene-containing agents are contained within the nitroaromatic subset. These molecules are under continuing investigation for their involvement in enzyme-catalyzed prodrug therapy, where endogenous enzymes activate (reduce) the nitro functional group to stimulate the formation of a cytotoxic, bioactive molecule. This is demonstrated by the hypoxia-selective antitumor arylmethyl quaternary mustard, *N,N-bis*(2-chloroethyl)-*N*-methyl-*N*-(2-nitrobenzyl)ammonium chloride (Figure 1d), which undergoes reductively induced fragmentation reactions via a radical intermediate.[16,17] Nitrobenzyl-containing rhenium and technetium complexes may be equally as effective as 2-nitroimidazole-based complexes.

An alternative to the $\{Tc^{V}O\}^{3+}$ core is the *fac*-$\{Tc^{I}(CO)_3\}^{+}$ precursor. Seminal developments in synthetic methods that allow the preparation of technetium compounds of the type *fac*-$[Tc(CO)_3(H_2O)_3]^{+}$ under conditions amenable to radiopharmaceutical applications have stimulated the focus on this approach and reinvigorated research into targeted technetium radiopharmaceuticals.[18] The "tricarbonyl core" approach exploits the stability of the metal tricarbonyl core while manipulating the relatively labile water ligands to attach targeting vectors. A variety of mono-, bi-, and tridentate ligands can react with the *fac*-$\{Tc^{I}(CO)_3\}^{+}$ fragment and displace the substitutionally labile aquo ligands.

The lack of nonradioactive isotopes of technetium complicates exploratory chemical synthesis. Consequently, rhenium, the nonradioactive, group VII congener of technetium, is often used as a ^{99m}Tc surrogate in developmental chemistry. Rhenium and technetium have similar ionic radii, and $\{M^{I}(CO)_3\}^{+}$ (M = Tc, Re) complexes are often isostructural. The interest in rhenium analogues also extends to the possibility of using the β^{-}-emitting rhenium isotopes ^{186}Re ($t_{1/2}$ = 90.6 h, E_{max} = 1.1 MeV, 91%) and ^{188}Re ($t_{1/2}$ = 17.0 h, E_{max} = 2.1 MeV, 85%) for radiotherapeutic applications.[19]

In this paper, we describe the synthesis and characterization of *fac*-$\{M^{I}(CO_3)\}^{+}$ (M = Re, ^{99m}Tc) complexes with aromatic amine bi- and tridentate ligands containing nitroaromatic functional groups with a view to producing hypoxia-selective agents. Aromatic amines coordinate to the metal ion with rapid complexation kinetics, and the resulting complexes possess high stability.[18] Though much emphasis has focused on the stability of tridentate chelators, the [2 + 1] mixed-ligand option may also be a viable approach due to the strong-field nature of the *fac*-$\{M^{I}(CO)_3\}^{+}$ (M = Tc, Re) core. A potential advantage of [2 + 1] mixed-ligand complexation is that the apical [+1] site can be changed to modulate the physical characteristics of the compound such as the solubility, lipophilicity, and ultimately membrane permeability.

The use of a single tridentate ligand has potential benefits in the ease of radiochemical synthesis as well as enhanced complex stability. Dipicolylamine,[20−23] picolylamine monoacetic acid,[23−25] and iminodiacetic acid[23,26,27] are commonly used tridentate ligands to form complexes with *fac*-$\{M^{I}(CO)_3\}^{+}$ (M = Tc, Re), and a series of iminodiacetic acid-based ligands featuring 2-nitroimidazole functional groups have been investigated as potential hypoxia tracers.[26−29]

In this study, a series of rhenium complexes containing either nitroaromatic or 2-nitroimidazole functional groups are prepared and characterized. The cell uptake of the rhenium compounds in both normoxia and under hypoxic conditions was investigated using inductively coupled plasma mass spectrometry (ICP-MS) and confocal fluorescence microscopy. The technetium-99m complexes have been prepared and characterized by comparison to the nonradioactive rhenium analogues and one example has been assessed in a hypoxic tumor model.

RESULTS AND DISCUSSION

Synthesis and Characterization of [2 + 1] Mixed-Ligand Ligands and Complexes. Two potentially bidentate, 2-pyridylhydrazone ligands, HL^1 and HL^2 (Figure 2), each bearing a nitro functional group, were prepared by condensation of 2-hydrazinopyridine with either *p*-nitrobenzaldehyde or *m*-nitrobenzaldehyde. The ligands were characterized by NMR spectroscopy, ESI-MS, and X-ray crystallography.

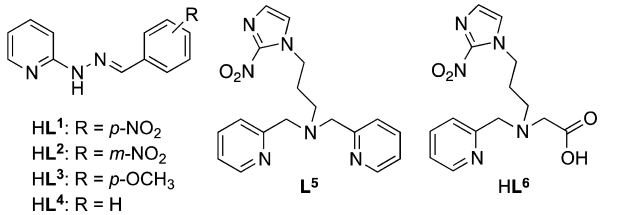

Figure 2. Bidentate ligands, HL^1−HL^4, and tridentate ligands, L^5 and HL^6.

DOI: 10.1021/acs.inorgchem.5b01691
Inorg. Chem. XXXX, XXX, XXX−XXX

X-ray crystallography of HL^1 and HL^2 (Figure 3) reveals that both compounds crystallize in the *E* conformation. ^{1}H NMR

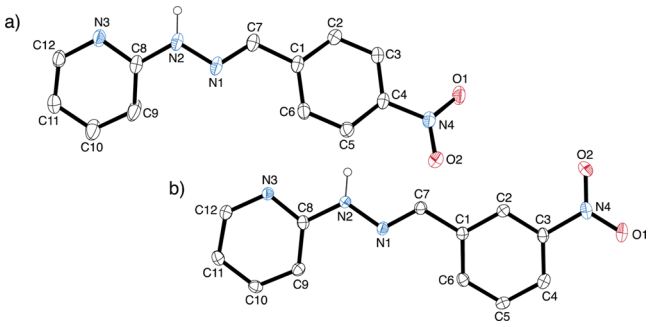

Figure 3. ORTEP representations of nitro-bearing ligands (a) HL^1 and (b) HL^2 with thermal ellipsoids shown at 50% probability. Hydrogen atoms have been omitted unless relevant.

spectroscopy suggests that this conformation is retained when HL^1 and HL^2 are dissolved in d_6-DMSO, as in both cases the hydrazinic proton atom gives a broad resonance at δ 10.4−11.3 ppm.

The $[NEt_4]_2[Re(CO)_3Br_3]$ precursor is commonly used to prepare complexes featuring a *fac*-$\{Re^I(CO)_3\}^+$ core and is often synthesized by reacting $[Re(CO)_5Br]$ with excess tetraethylammonium bromide in diglyme at 180 °C. An alternative starting material, *fac*-$[Re(CO)_3(H_2O)_3]^+$, can be prepared by heating $[Re(CO)_5Br]$ at reflux in water for 24 h. This more convenient method is moderately successful, but the relative insolubility of the $[Re(CO)_5Br]$ starting material in water and its hydrophobicity leads to a substantial loss in yield when working on smaller scales (ca. < 100 mg) as the rhenium pentacarbonyl bromide tends to coat glassware and require constant "washing" back into the reaction mixture. During the course of this work, we have developed a microwave heating method of producing *fac*-$[Re(H_2O)_3(CO)_3]^+$ in near quantitative yields that is equally effective on small scales as on larger scales. Commercially available $[Re(CO)_5Br]$ was suspended in water and the mixture sparged with nitrogen and subjected to microwave-assisted thermal heating for three intervals of 10 min to give clear solutions of *fac*-$[Re(CO)_3(OH_2)_3]Br$ in essentially quantitative yields and significantly reduced reaction times (Scheme 1).

Complexes *fac*-$[Re(CO)_3(HL^1)Br]$ and *fac*-$[Re(CO)_3(HL^2)Br]$ were synthesized by the addition of equimolar amounts of the ligands to a mixture of *fac*-$[Re(CO)_3(OH_2)_3]Br$ in methanol (Scheme 1). The major signal in the high resolution ESI-MS of both complexes, with the predicted isotope pattern, was for the cation formed by a loss of coordinated bromide at m/z = 513.0203 (calculated 513.0203). The resonances attributed to the hydrazinic N*H* proton in the ^{1}H NMR spectra of the complexes *fac*-$[Re(CO)_3(HL^1)Br]$ and *fac*-$[Re(CO)_3(HL^2)Br]$ are shifted downfield when compared to the "free" ligands, for example, N*H*(hydrazinic) δ 13.2 ppm for *fac*-$[Re(CO)_3(HL^1)Br]$ compared to δ 9.84 ppm for HL^1. The structures of *fac*-$[Re(CO)_3(HL^1)Br]$ and *fac*-$[Re(CO)_3(HL^2)Br]$ were confirmed by X-ray crystallography (Figure 4).

Replacing the monodentate [+1] bromide ligand can lead to the modification of physical and biological properties of the metal and also produce complexes that are more resistant to substitution *in vivo*. It was of interest to use pyridine based ancillary [+1] ligands due to the ability of heterocyclic amines to form complexes that are resistant to substitution, and the use of 3-(dimethylamino)-1-propylamine (DMAPA) as an ancillary ligand was designed to dramatically change solubility and membrane permeability.

Initial synthesis used a high-boiling solvent, 1,2-dichlorobenzene, and an excess of ligand. A superior synthetic procedure involved the reaction of equimolar amounts of ligand, HL^1 or HL^2, and *tris*-substituted *fac*-$[Re(CO)_3(X)_3]^+$ (X = pyridine, 4-picoline, 3-(dimethylamino)-1-propylamine) in methanol via microwave irradiation for 20 min (Scheme 1). Crystals of *fac*-$[Re(CO)_3(L^{1-2})(X)]$, suitable for X-ray analysis, were formed following partial evaporation of the reaction mixture solvent, in yields of approximately 70% (Figure 5, Table 4). Replacing the monodentate bromide ligand with basic *N*-containing heterocycles, pyridine or 4-picoline, resulted in the isolation of neutral complexes with the deprotonation of the bidentate hydrazone ligand.

It is interesting to note that *fac*-$[Re(CO)_3(HL^1)(pyridine)]BPh_4$ is the only complex to crystallize as the cationic species via protonation of the hydrazinic (N2) nitrogen (Figure 5a); nonetheless deprotonation is easily induced by the addition of

Scheme 1. Reaction Schemes for the Synthesis of *fac*-$[Re(CO)_3(OH_2)_3]Br$, *fac*-$[Re(CO)_3(HL^{1-4})Br]$, and *fac*-$[Re(CO)_3(L^{1-2})(X)]$ (X = pyridine, 4-picoline, DMAPA) Complexes

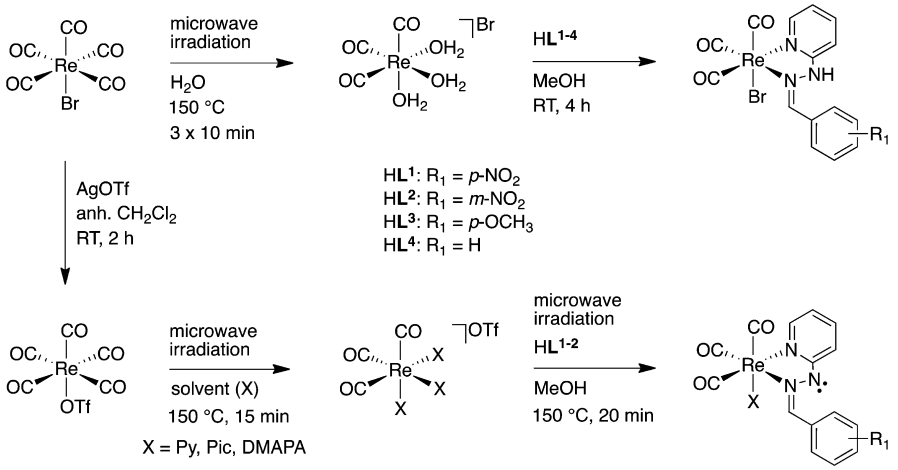

DOI: 10.1021/acs.inorgchem.5b01691
Inorg. Chem. XXXX, XXX, XXX−XXX

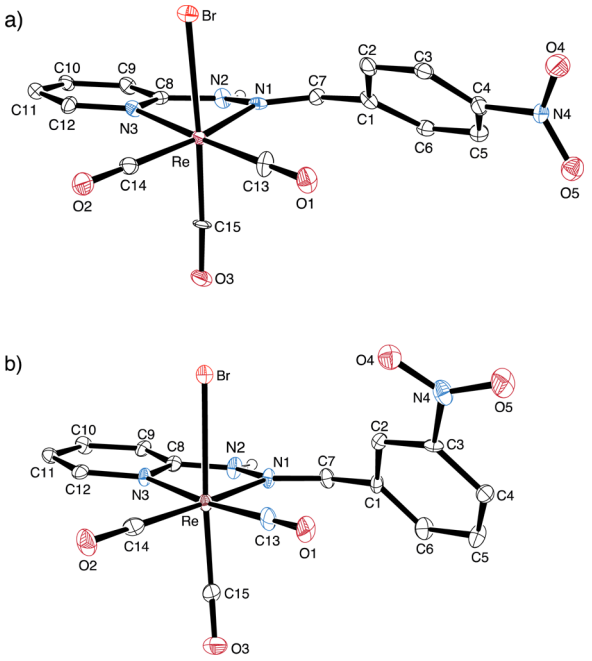

Figure 4. ORTEP representations of complexes (a) *fac*-[Re(CO)$_3$(HL^1)Br] and (b) *fac*-[Re(CO)$_3$(HL^2)Br], with thermal ellipsoids shown at 50% probability. Hydrogen atoms have been omitted unless bound to nitrogen.

triethylamine. The differences between the protonated and nonprotonated N2 derivatives are exemplified in the C1−C7−N1−Re torsion angles, whereby the cationic complex *fac*-[Re(CO)$_3$(HL^1)(pyridine)]$^+$ possesses an angle of 19.0(8)°, and torsion angles for the three complexes deprotonated at the N2 nitrogen (*fac*-[Re(CO)$_3$(L^2)(pyridine)] and *fac*-[Re(CO)$_3$(L^{1,2})(4-picoline)]) lie between 174.4 and 179.0° (Figure 5, Table 1).

The Re−N4 bond lengths are predictably shorter than the Re−Br distances for the *fac*-[Re(CO)$_3$(HL$^{1-2}$)(Br)] series of complexes, with an average distance of 2.626 Å for the two nitro-substituted *fac*-[Re(CO)$_3$(HL$^{1-2}$)(Br)] complexes and 2.212 Å for the *N*-heterocycle substituted complexes (Table 1). Additionally, the Re−N1 distance is also consistently shorter for complexes with nitroaromatic coordination at the ancillary site, compared to the bromo-substituted rhenium complexes (2.22 vs 2.16 Å).

The N1−C7 sp^2 hybridized bond for the two nitro-bearing ligands (HL$^{1-2}$) in (*fac*-[Re(CO)$_3$(L$^{1-2}$)Br]) and *fac*-[Re(CO)$_3$(L$^{1-2}$)(X)] (X = pyridine, 4-picoline) does not vary significantly in length. The N1−C7 distances for ligands HL^1 and HL^2 are 1.278(2) and 1.279(3) Å, respectively. A slight increase in this bond length is observed upon coordination as the apical, monodentate ligand is varied from bromo, pyridine, or picoline coordination. For all neutral, [2 + 1] complexes without a coordinated bromide, the Re−N1 bonds of the five-membered chelate ring are shorter (2.16 vs 2.22 Å), and Re−N3 and C8−N3 bond lengths are longer when compared to the analogous complexes with a coordinated anionic bromide (1.37 vs 1.34 Å). N1−N2 bond lengths of *fac*-[Re(CO)$_3$(HL^1)(Br)] and *fac*-[Re(CO)$_3$(L^1)(4-picoline)] (average 1.356 Å) tend toward the distance of the N1−N2 ligand bond (average 1.358

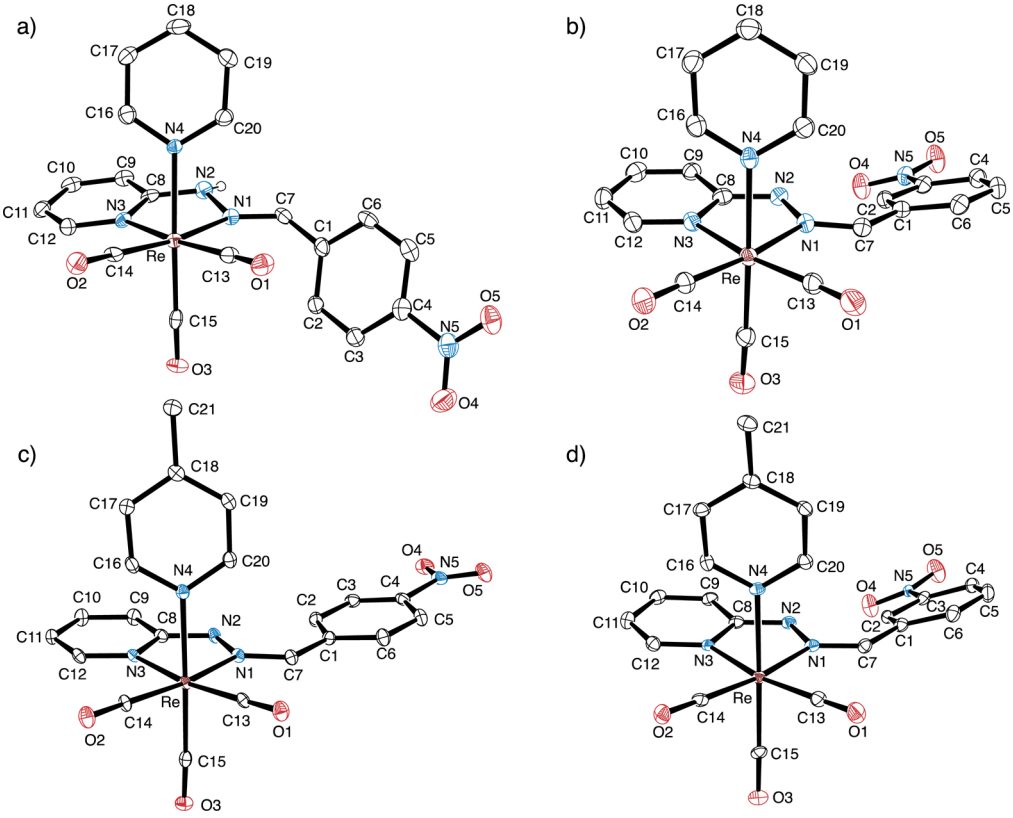

Figure 5. ORTEP representations of (a) *fac*-[Re(CO)$_3$(HL^1)(pyridine)]BPh$_4$, (b) *fac*-[Re(CO)$_3$(L^2)(pyridine)], (c) *fac*-[Re(CO)$_3$(L^1)(4-picoline)], (d) *fac*-[Re(CO)$_3$(L^2)(4-picoline)] with thermal ellipsoids shown at 50% probability. Hydrogen atoms, counterion, and solvent molecules have been omitted for clarity unless relevant.

DOI: 10.1021/acs.inorgchem.5b01691
Inorg. Chem. XXXX, XXX, XXX−XXX

Table 1. Selected Bond Lengths (Å) and Angles (deg) for (1) *fac*-[Re(CO)$_3$(HL^1)(pyridine)]BPh$_4$ (2) *fac*-[Re(CO)$_3$(L^2)(pyridine)] (3) *fac*-[Re(CO)$_3$(L^1)(4-picoline)] (4) *fac*-[Re(CO)$_3$(L^2)(4-picoline)][a]

	1	2	3	4
bond lengths				
Re−N(4)	2.201(4)	2.217(5)	2.216(3)	2.215(4)
Re−N(1)	2.165(4)	2.161(4)	2.159(3)	2.155(4)
Re−N(3)	2.195(4)	2.134(4)	2.134(3)	2.147(4)
Re−C(13)	1.932(6)	1.935(5)	1.919(4)	1.936(5)
Re−C(14)	1.937(5)	1.905(5)	1.932(3)	1.912(4)
Re−C(15)	1.909(6)	1.921(6)	1.931(4)	1.923(5)
N(1)−N(2)	1.379(6)	1.380(5)	1.354(4)	1.379(5)
N(2)−C(8)	1.362(7)	1.329(6)	1.351(5)	1.342(6)
N(3)−C(8)	1.361(6)	1.374(7)	1.365(5)	1.376(6)
N(1)−C(7)	1.294(6)	1.295(6)	1.319(5)	1.319(6)
bond angles				
N(1)−Re−N(3)	75.15(16)	74.08(15)	73.89(12)	74.25(14)
N(3)−Re−C(14)	99.79(18)	98.97(19)	97.47(14)	98.07(17)
C(14)−Re−C(13)	90.6(2)	87.6(2)	88.09(15)	86.42(19)
C(13)−Re−N(1)	100.1(2)	98.55(18)	98.57(13)	96.45(17)
C(13)−Re−N(3)	174.6(2)	172.18(18)	171.42(13)	169.95(17)
C(14)−Re−N(1)	172.67(18)	172.83(19)	171.20(13)	171.72(17)
C(15)−Re−N(4)	174.65(19)	176.4(2)	177.44(13)	177.53(16)
C(14)−Re−N(4)	94.00(18)	93.86(19)	92.30(14)	91.33(17)
C(13)−Re−N(4)	93.78(19)	93.57(19)	92.42(14)	92.00(17)
N(1)−Re−N(4)	80.20(16)	83.70(15)	85.03(11)	84.81(13)
N(3)−Re−N(4)	82.80(15)	83.15(15)	82.95(11)	83.50(13)
C(13)−Re−C(15)	89.3(2)	89.7(2)	90.12(15)	87.0(2)
C(14)−Re−C(15)	90.6(2)	87.6(2)	88.09(15)	86.42(19)
C(15)−Re−N(1)	94.95(19)	94.45(19)	94.21(14)	97.56(16)
C(15)−Re−N(3)	93.81(18)	93.4(2)	94.49(13)	97.81(16)

[a]Complexes are listed in order of appearance from Figure 5.

Å), while all other complexes consistently show slightly longer lengths (between 1.379 and 1.382 Å).

The ^{1}H NMR spectra of the ligand and complexes with an *m*-nitro substituent (HL^2, *fac*-[Re(CO)$_3$(HL^2)(Br)], *fac*-[Re(CO)$_3$(L^2)(4-picoline)], *fac*-[Re(CO)$_3$(L^2)(pyridine)], and *fac*-[Re(CO)$_3$(L^2)(DMAPA)]) were all as expected. For example, coordination of the metal ion to HL^2 results in a significant downfield shift in the resonance attributed to the proton attached to C2 (Figure 4b), shifting from δ 8.47 ppm for HL^2 to δ 9.66 ppm for the complex *fac*-[Re(CO)$_3$(L^2)(4-picoline)]. Additionally, for all picoline, pyridine, and DMAPA complexes, a dramatic shift to a higher field for the resonance attributed to the C*H*═N proton is observed. As this shift is not reflected in the bromo complexes, it can be assumed that the shielding effects of the nitrogen-containing moiety are substantial.

The resonance of the hydrazinic N*H* signals in the proton NMR of the ligands and *fac*-[Re(CO)$_3$(HL$^{1-4}$)(Br)] complexes demonstrate a shift upfield once the ligand coordinates the metal; for instance, the "free" ligand HL^1 displays an N*H* resonance at δ 9.84 ppm which shifts to δ 13.2 ppm for the complex *fac*-[Re(CO)$_3$(HL^1)Br]. Hydrazinic proton shifts are not evident for the picoline, pyridine, or DMAPA complexes, and the absence of the hydrazinic υ(N−H) infrared stretch, which is apparent in the protonated complexes between $\bar{\nu}$ 3182 and 2931 cm^{-1}, provides support that these complexes are deprotonated.

Infrared C═H stretches for the monodentate pyridine ring and the azomethine are shifted to a slightly higher energy compared to the "free" ligand, which is consistent with the decrease in electron density within the rings and backbone, though overlap of the absorbances from the pyridine skeletal bands and υ(NO$_2$) stretches cause some obscurity.

The infrared spectra for *fac*-[Re(CO)$_3$(H$_2$O)$_3$]$^+$ and the *tris*-picoline and *tris*-pyridine complexes consistently display two typical stretching bands for the facially orientated terminal tricarbonyl, υ(C≡O), moiety at $\bar{\nu}$ 2040 and 1881 cm^{-1}. All other complexes which deviate from C_{3v} symmetry show either two or three bands between $\bar{\nu}$ 2016 and 1894 cm^{-1} in the typical carbonyl stretching region of compounds containing α-diimine ligands.[30] It is assumed that those complexes which display only two stretches have the middle band obscured by the stronger, broad stretch at the lower energy.

Electrochemical Studies. The electrochemical characteristics of the nitro-containing ligands (HL^1 and HL^2) and all [2 + 1] mixed-ligand complexes were studied by cyclic voltammetry in acetonitrile. Potentials are quoted relative to the ferrocene/ferrocenium couple, where $E^{0\prime}$ is designated as +0.40 V vs SCE.[31] The cathodic region was investigated for all compounds in order to establish the location of significant redox processes. Comparative redox potentials were examined against the *para*-methoxy substituted complex *fac*-[Re(CO)$_3$(L^3)Br] and unsubstituted phenyl derivative *fac*-[Re(CO)$_3$(L^4)Br] (where R$_1$ = −OCH$_3$ or −H).

For nitro-containing complexes *fac*-[Re(CO)$_3$(HL^1)Br] and *fac*-[Re(CO)$_3$(HL^2)Br], two reduction waves are observed within the range 0.0 and −1.15 V. The first peak is generally irreversible and the second quasi-reversible; this is a common observation for nitro-aromatic compounds,[32,33] although this pattern was not seen for either of the nitro-based ligands which display only one quasi-reversible peak.

Complexes containing the nitro substituent in the *para* position of the ligand (L^1) consistently display higher reduction potentials and more complex voltammograms than the *meta*-nitro (L^2) species. The broadness of the first reduction wave for *fac*-[Re(CO)$_3$(L$^{1-2}$)Br] and *fac*-[Re(CO)$_3$(L^2)(X)] (X = pyridine, 4-picoline) indicates that multiple electron processes are occurring. This is further confirmed by the occurrence of three distinct reduction peaks for *fac*-[Re(CO)$_3$(L^1)(pyridine)] between −0.80 and −1.18 V (Table 2).

It is worth noting that complexes with nitrogen substituted [+1] ancillary ligands are deprotonated at the hydrazinic nitrogen in solution, if not confirmed by the crystal structure data but also by the change in color to the analyte solution to deep red. This indicates that the first cathodic peak most likely involves a proton-coupled reduction, which, though ligand based, is affected by coordination to the metal to give an electrochemical−chemical based process.

DOI: 10.1021/acs.inorgchem.5b01691
Inorg. Chem. XXXX, XXX, XXX−XXX

Table 2. Electrochemical Data for Selected Ligands and Complexes[a]

	E_{pc1} (V)[b]	$E_{pc(qr)}$ (V)[c]	$i_{pa(qr)}/i_{pc(qr)}$[d]	ΔE_p (mV)[e]
HL^1		−1.10	3.38	58
HL^2		−1.18	3.00	58
fac-[$Re(CO)_3(HL^1)Br$]	−0.65	−1.05	0.87	62
fac-[$Re(CO)_3(HL^2)Br$]	−0.74	−1.14	1.38	64
fac-[$Re(CO)_3(HL^3)Br$]	−1.50			
fac-[$Re(CO)_3(HL^4)Br$]	−1.32			
fac-[$Re(CO)_3(L^1)$(4-pic)]		−0.98	0.74	60
fac-[$Re(CO)_3(L^1)$(py)]	−0.80	−0.99 (−1.18)[f]	0.90	64
fac-[$Re(CO)_3(L^2)$(4-pic)]	−0.71 (−0.85)[f]	−1.14	1.29	63
fac-[$Re(CO)_3(L^2)$(py)]	−0.81	−1.13	0.87	56

[a]Potential measurements of all complexes are referred to the SCE, with 1.0 mM analyte in CH_3CN/100 mM [Bu_4N][BF_4] relative to the Fe^0/Fe^1 redox couple, $E^{0\prime}$ = +0.40 V (vs SCE) at a 100 mV s^{-1} scan rate [b]Cathodic peak potential corresponding to the first reduction step. Where there is no value given, the first cathodic peak is quasi-reversible, and values are provided in the proceeding column. [c]Cathodic peak potential corresponding to the second quasi-reversible (qr) reduction step. [d]Peak current ratio of second quasi-reversible cathodic peak. [e]$\Delta E_p = |E_{pc} - E_{pa}|$ of quasi-reversible peak (voltage separation between current peaks). [f]Potentials in brackets indicate a visibly distinct reduction potential between or after indicated reduction peaks. Abbreviations: pc = cathodic potential, pa = anodic potential, qr = quasi reversible.

The latter, quasi-reversible cathodic peak is assigned to an initial one-electron reduction of the nitro conjugate base to the radical anion.[5,7,32,34] All quasi-reversible reduction processes show a peak separation (ΔE_p) value between 58 and 64 mV indicating a one-electron reversible process. Peak current ratios (i_p/i_a) are more variable, with ratios for the complex quasi-reversible reduction processes between 0.74 and 1.38. All quasi-reversible reduction processes for the rhenium complexes were measured at scan rates of 50, 100, 200, and 300 mV s^{-1} and produce linear correlations ($R^2 \approx 0.99$) when plotted against the square root of the scan rate ($v^{1/2}$).

The redox chemistry for the *meta*-nitro ligand (HL^2) compared to corresponding rhenium complexes displays a slight shift to higher potential values upon coordination, whereby the uncomplexed ligand shows an E_{pc} value of −1.18 V and the complexes have reduction potentials of −1.14 V (Figure 6); this is tentatively assigned to the slightly electron-withdrawing nature of the metal center.[7]

For similar rhenium compounds, the metal-centered reduction assigned to Re^1/Re^0 is between −1.2 and −1.6 V and devoid of an oxidation wave (CH_3CN, 100 mM tetrabutylammonium perchlorate).[35] It is most likely that, within the observed window, experimental potentials are not inclusive of the reduction of rhenium. Furthermore, the reduction of rhenium(I) to rhenium(0) is not likely to occur in the cellular environment.

Synthesis and Characterization of Tridentate Ligands and Complexes. The preparation of the ligands involved in the formation of the two tridentate complexes *fac*-[$Re(CO)_3(L^5)$]BPh_4 and *fac*-[$Re(CO)_3(L^6)$] took advantage of the previously reported synthesis of 2-nitroimidazole by initial diazatization from 2-aminoimidazole sulfate, and subsequent nitration was performed using copper sulfate as a catalyst.[36] Bromoalkylation of the potassium salt of the nitroimidazole was obtained according to published procedure using 18-crown-6 in anhydrous acetonitrile to afford the desired bromobutylimidazole (**1**).[37]

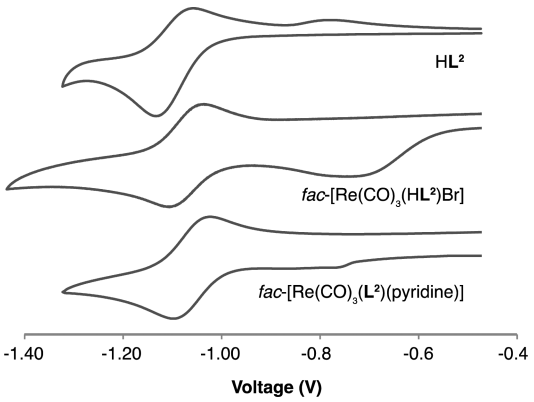

Figure 6. Cyclic voltammograms of selected *meta*-NO_2 compounds. Experimental conditions: 1.0 mM analyte in 100 mM [tBu_4N][BF_4]/CH_3CN electrolyte solution, scan rate 100 mV s^{-1}.

Formation of the tridentate ligand, L^5, involved a substitution reaction of bromoalkylated nitroimidazole **1** with di(2-picolyl)-amine and *N*,*N*-diisopropylethylamine (DIPEA) as a base. A solution of ligand L^5 and [$Re(CO)_5OTf$] in methanol was subjected to microwave irradiation at 120 °C for 15 min and precipitated with sodium tetraphenylborate in methanol, resulting in the formation of the desired complex *fac*-[$Re(CO)_3(L^5)$]BPh_4. The complex was crystallized by evaporation of a solution of the complex in methanol, to afford clear, block crystals in a moderate yield (56%; Scheme 2).

A similar procedure for the formation of the neutral complex *fac*-[$Re(CO)_3(L^6)$] was used; however synthesis of the ligand, HL^6, involved the initial preparation of **2** via condensation of 2-picolylamine and ethylbromoacetate followed by Kugelrohr distillation and reaction with the bromoalkylated nitroimidazole, **1**. *In situ* hydrolysis of the ester using sodium hydroxide and thermal heating at 120 °C with [$Re(CO)_5OTf$] in acetonitrile afforded the desired complex *fac*-[$Re(CO)_3(L^6)$], in good yield as an off-white solid (76%).

High resolution ESI mass spectrometry of both ligands, L^5 and HL^6, indicates consistency with all spectroscopic data; for instance, the pure ligand, L^5, was obtained with an *m*/*z* peak at 353.1723, assigned to $[L^5+H]^+$ (calculated 353.1726). Both complexes clearly show the rhenium isotopic pattern at their expected *m*/*z* peaks.

IR spectra of both tridentate complexes demonstrate stretching bands between $\bar{\nu}$ 2027 and $\bar{\nu}$ 1874 cm^{-1}, indicating the presence of the *fac*-{$Re(CO)_3$}$^+$ core. The carbonyl stretch for the esterified ligand, L^6Et ($\bar{\nu}$ 1730 cm^{-1}), is within the typical range,[38] but upon complexation a reduced frequency of absorption is observed for the neutral complex *fac*-[$Re(CO)_3(L^6)$], with absorptions at $\bar{\nu}$ 1652 and 1365 cm^{-1}. These two bands are believed to denote carboxylate asymmetrical and symmetrical stretching bands, $\upsilon_{as}(C\overset{\cdots}{=}O)_2^-$ and $\upsilon_s(C\overset{\cdots}{=}O)_2^-$ respectively, and are not seen for the cationic structure *fac*-[$Re(CO)_3(L^5)$]$^+$.

DOI: 10.1021/acs.inorgchem.5b01691
Inorg. Chem. XXXX, XXX, XXX−XXX

Scheme 2. Synthesis of Tridentate Complexes *fac*-$[Re(CO)_3(L^5)]^+$ and *fac*-$[Re(CO)_3(L^6)]$

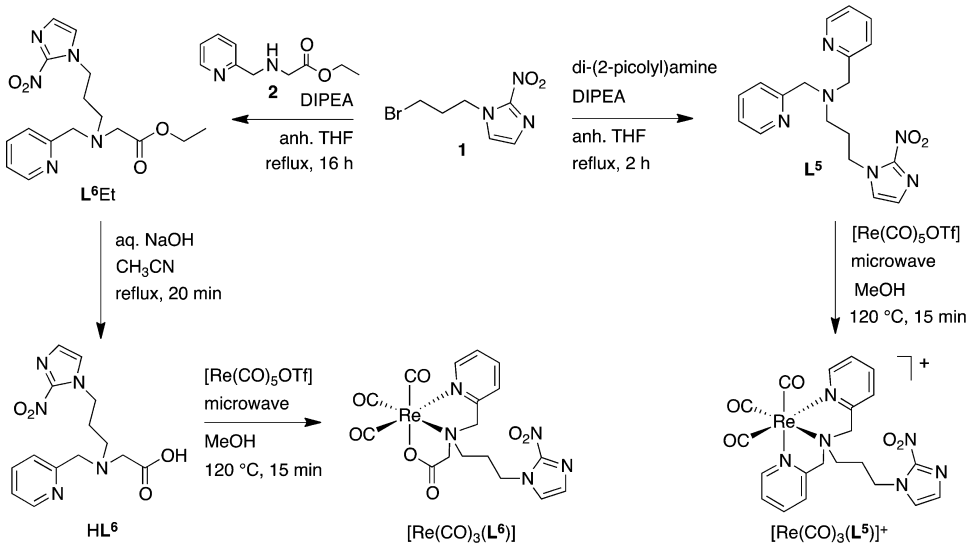

Coordination of the *fac*-$\{Re(CO)_3\}^+$ core to L^5 results in a significant downfield shift in resonances in both the ^1H and $^{13}C\{^1H\}$ NMR spectra, particularly for the equivalent methylene protons adjacent to the pyridine rings which shift from a singlet resonance at δ 3.74 ppm for the ligand to δ 4.60 ppm for the complex; this is most likely due to the deshielding effects of the rhenium center. Similar patterns are observed for the HL^6 ligand and complex. Evidence advocating the formation of the neutral complex shows transformation of the methylene protons adjacent to the pyridine and carboxylate from two singlet resonances to a distinctive set of four doublets indicating geminal coupling ($^2J_{HH}$ = 16 Hz); this does not occur for the cationic complex.

Crystals suitable for analysis by X-ray crystallography for *fac*-$[Re(CO)_3(L^5)]BPh_4$ were grown from a concentrated solution of the compound in methanol (Figure 7). The complex

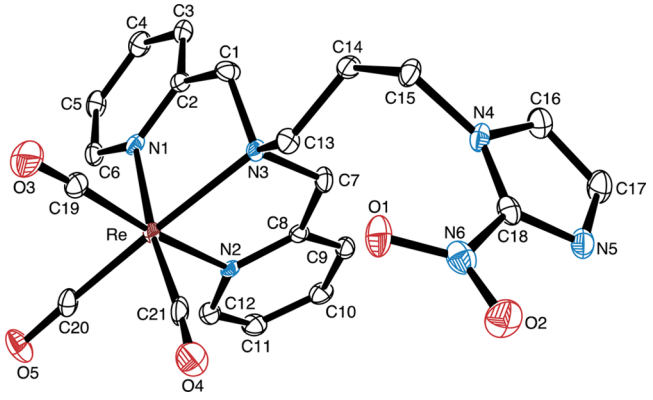

Figure 7. ORTEP representation of *fac*-$[Re(CO)_3(L^5)]^+$ with thermal ellipsoids shown at 50% probability. Hydrogen atoms, counterion, and solvent molecules have been omitted for clarity.

crystallizes in the triclinic space group, $P\bar{1}$, and displays characteristic crystallographic parameters, bond lengths and angles for a tricarbonyl, tridentate rhenium complex (Table 3, Table 4).[25,26,39]

Cyclic voltammetry shows a reduction peak pattern similar to those seen for the [2 + 1] mixed-ligand complexes. A quasi-reversible cathodic peak was observed at −1.10 and −1.11 V for

Table 3. Selected Bond Lengths (Å) and Angles (deg) for the Rhenium Complex *fac*-$[Re(CO)_3(L^5)]^+$[a]

Bond Lengths					
Re–C(19)	1.927(3)	Re–N(1)	2.184(3)	C(19)–O(3)	1.147(4)
Re–C(20)	1.913(3)	Re–N(2)	2.165(2)	C(20)–(O5)	1.152(4)
Re–C(21)	1.922(4)	Re–N(3)	2.227(2)	C(21)–(O4)	1.151(4)
Bond Angles					
N(1)–Re–C(21)		173.63(10)	N(1)–Re–N(3)		77.34(9)
N(2)–Re–C(19)		174.03(12)	N(1)–Re–N(2)		78.30(9)
N(3)–Re–C(20)		173.52(10)	N(3)–Re–N(2)		78.36(9)
C(19)–Re–N(1)		96.18(12)	C(20)–Re–N(1)		99.03(12)
C(19)–Re–N(3)		98.33(11)	C(20)–Re–N(2)		95.70(110
C(19)–Re–C(21)		85.48(14)	C(20)–Re–C(21)		87.18(13)

[a]Bond distances and angles for the Ph_4B counterion have not been shown.

both nitro ligand species, L^5 and L^6Et, respectively. The quasi-reversible reduction wave for the complexes is shifted to −1.08 V for the cationic *fac*-$[Re(CO)_3(L^5)]^+$ complex and −1.12 V for *fac*-$[Re(CO)_3(L^6)]$. No initial, nonreversible reduction peak was observed for the complexes, suggesting that any other reduction processes occur outside of the observed window.

UV–Visible and Fluorescence Studies. The absorption spectra of both HL^1 and HL^2 dissolved in acetonitrile display two peaks in the UV region, HL^1 at λ 387 and 254 nm and HL^2 at λ 327 and 225 nm, and are assigned to $\pi \rightarrow \pi^*$ transitions. In the metal complexes featuring a *meta*-nitro functional group, MLCT transitions at λ 463–469 nm are evident that shift to λ 520–528 nm for complexes possessing the *para*-NO_2 functional group. These values reflect those of similar low-valent, rhenium complexes, albeit more often as the α-diimine rather than the hydrazone functionality.[40] The low energy absorbance demonstrates the strong π acceptor nature of the ligands, and the bathochromic shift of the *para*-NO_2 complexes implies the delocalization of electron density caused by the *para* substituent.

Complexes where the pyridyl-hydrazone is deprotonated and contains the *para*-NO_2 substituent *fac*-$[Re(CO)_3(L^1)(X)]$ (X =

DOI: 10.1021/acs.inorgchem.5b01691
Inorg. Chem. XXXX, XXX, XXX–XXX

Table 4. Summary of Crystal Data and Structure Refinement for Selected Complexes (1) HL^1, (2) HL^2, (3) *fac*-$[Re(CO)_3(HL^1)Br]$, (4) *fac*-$[Re(CO)_3(HL^2)Br]$, (5) *fac*-$[Re(CO)_3(L^1)(4\text{-picoline})]$, (6) *fac*-$[Re(CO)_3(L^2)(4\text{-picoline})]$, (7) *fac*-$[Re(CO)_3(HL^1)(pyridine)]BPh_4$, (8) *fac*-$[Re(CO)_3(L^2)(pyridine)]$, (9) *fac*-$[Re(CO)_3(L^5)]BPh_4$

	1[a]	2[a]	3[b]	4[b]	5[b]	6[c]	7[d]	8[c]	9[b]
formula	$C_{12}H_{10}N_4O_2$	$C_{12}H_{10}N_4O_2$	$C_{15}H_{10}BrN_4O_5Re$	$C_{15}H_{10}BrN_4O_5Re$	$C_{23}H_{19}N_6O_5Re$	$C_{22}H_{16}N_4O_5Re$	$C_{45}H_{39}BN_5O_6Re$	$C_{20}H_{14}N_5O_5Re$	$C_{45}H_{40}BN_6O_5$ Re
fw	242.24	242.24	592.38	592.38	645.64	605.59	942.82	590.56	941.84
size (mm^3)	0.33 × 0.09 × 0.03	0.50 × 0.09 × 0.07	0.1 × 0.05 × 0.04	0.16 × 0.05 × 0.02	0.21 × 0.14 × 0.01	0.3 × 0.09 × 0.04	0.22 × 0.09 × 0.03	0.50 × 0.50 × 0.40	0.72 × 0.57 × 0.39
system	triclinic	monoclinic	triclinic	triclinic	monoclinic	monoclinic	monoclinic	orthorhombic	triclinic
space group	$P\bar{1}$	$C2/c$	$P\bar{1}$	$P\bar{1}$	$P2_1/c$	$P2_1/c$	$P2_1/n$	$Pbca$	$P\bar{1}$
T (K)	130.0(2)	130.0(2)	130.0(2)	130.0(2)	130.0(2)	130.0(2)	130.0(2)	130.0(2)	130.0(2)
λ (Å)	1.5418	1.5418	1.5418	1.5418	1.5418	1.5418	1.5418	1.5418	1.5418
a (Å)	4.5731(3)	23.9942(8)	7.0457(4)	6.7204(16)	18.1762(3)	16.4614(2)	11.99950(10)	8.050(2)	9.6870(3)
b (Å)	10.1399(5)	5.5373(2)	7.2712(5)	10.010(2)	9.21900(10)	7.75170(10)	22.9282(2)	15.143(4)	11.9283(3)
c (Å)	11.9298(6)	16.7262(6)	16.6373(6)	13.421(3)	14.1755(2)	16.0826(2)	14.58840(10)	32.934(8)	17.5604(5)
α (deg)	84.316(4)	90	77.386(5)	98.322(18)	90	90	90	90	82.240(2)
β (deg)	89.360(4)	97.034(3)	88.360(5)	98.896(19)	99.434(2)	91.4930(10)	95.6580(10)	90	78.321(2)
γ (deg)	87.516(4)	90	86.942(5)	101.067(19)	90	90	90	90	83.106(2)
V ($Å^3$)	549.94(5)	2205.5(13)	830.46(8)	861.1(3)	2343.21(6)	2051.50(4)	3994.11(6)	4014.8(18)	1959.88(10)
Z	2	8	2	2	4	4	4	8	2
D_{calcd} (Mg m^{-3})	1.463	1.459	2.369	2.038	1.830	1.951	1.568	1.954	1.596
μ (mm^{-1})	0.867	0.865	17.476	16.749	10.556	11.972	6.410	6.097	3.156
$F(000)$	252	1008	556	488	1256	1164	1888	2272	944
reflections measured	7509	3787	4628	4566	6664	7332	16352	22226	16002
independent reflections	2169	1986	2947	3024	4169	3693	7194	3532	6897
R [$I > 2\sigma(I)$]	0.0302	0.0386	0.0450	0.0494	0.0212	0.0332	0.0500	0.0546	0.0464
wR (F^2; all data)	1.042	1.111	1.078	1.114	1.020	1.018	0.884	1.097	1.027

[a]Crystals were grown from a concentrated solution of the compound in DMSO. [b]Crystals were grown from a concentrated solution of the compound in CH_3CN. [c]Crystals were grown via slow diffusion of Et_2O into a concentrated solution of the complex in CH_3OH. [d]Crystals were grown from a concentrated solution of the complex in CH_3OH and excess $NaBPh_4$.

DOI: 10.1021/acs.inorgchem.5b01691
Inorg. Chem. XXXX, XXX, XXX−XXX

4-picoline, pyridine, DMAPA) are luminescent, whereas *meta*-nitro species are not. The red-purple, *para*-nitro-substituted complex *fac*-[Re(CO)$_3$(**L^1**)(pyridine)] absorbs at a wavelength of 520 nm, with an emission at λ 715 nm (Figure 8). These

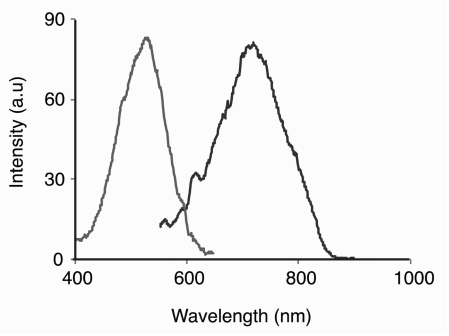

Figure 8. Excitation and emission spectra for *para*-nitro-bearing complex *fac*-[Re(CO)$_3$(**L^1**)(pyridine)] emission (λ_{ex} = 520 nm, light gray) and excitation (λ_{em} = 715 nm, dark gray): 25 μM, acetonitrile.

broad maxima are assigned to ^{3}MLCT states, which is a characteristic excited state nature of rhenium(I) polypyridine complexes.[41,42] Though Stokes' shifts are generally high in such cases, the [2 + 1], hydrazone-ligand coordination compounds presented here demonstrate larger Stokes' values than commonly observed (λ = 185−195 nm).

Deprotonation of the *fac*-[Re(CO)$_3$(H**L^1**)(Br)] and *fac*-[Re(CO)$_3$(H**L^1**)(pyridine)]BPh$_4$ complexes by the addition of triethylamine augmented emission intensity, which indicates that deprotonation for these complexes is not complete in acetonitrile despite the immediate changes in color from yellow to purple without the addition of a base.

The luminescence properties of such compounds may be useful for developmental investigations into cell localization and, due to their low energy emissions, are particularly beneficial to distinguishing between endogenous fluorophores, which typically emit at much higher energies.

Confocal Fluorescence Microscopy and ICP Mass Spectrometry. The luminescence properties of these complexes are useful for investigating cell uptake and intracellular localization using confocal fluorescent microscopy, as their relatively low energy excitation profiles and large Stokes' shifts allow images to be acquired with little autofluorescence due to endogenous fluorophores.[42−45]

A proof-of-concept study identified that it was possible to monitor cell uptake and distribution of the picoline-derived *fac*-[Re(CO)$_3$(**L^1**)(4-picoline)] complex within a HeLa cancer cell line with the aid of fluorescence microscopy. The cells were exposed to increasing concentrations of the compound (5−50 μM) for 30 min, and fluorescence was measured following excitation at a wavelength of 520 nm. The complex localizes primarily within the cytosol with no uptake in the nucleus. The complex also accumulated in puncta indicative of cytosolic vesicles, and the cells retained their morphology during the 30 min incubation (Figure 9).

The cellular permeability and retention of *fac*-[Re(CO)$_3$(H**L^1**)Br], *fac*-[Re(CO)$_3$(**L^1**)(4-picoline)], *fac*-[Re(CO)$_3$(**L^1**)(DMAPA)], and *fac*-[Re(CO)$_3$(**L^5**)]BPh$_4$ was assessed in human neuroblastoma SH-(SY5Y) cells. The cells were grown to 90% confluency, then incubated at 37 °C for 1 h, with a total rhenium complex concentration of 10 μM maximum. The intracellular rhenium concentrations were determined using ICP-MS. Basal rhenium levels were negligible in the DMSO vehicle control and 0.06 μM for the standard, rhenium-triflate complex [Re(CO)$_5$(CF$_3$SO$_3$)]. Significant increases in intracellular rhenium levels for all samples are observed when compared to either the DMSO vehicle treatment or the rhenium control. Cells treated with the tridentate complex *fac*-[Re(CO)$_3$(**L^5**)]BPh$_4$ revealed intracellular rhenium concentrations of 0.236 μg per milligram of protein. The [2 + 1] series of complexes, *fac*-[Re(CO)$_3$(**L^1**)(4-picoline)], *fac*-[Re(CO)$_3$(**L^1**)(DMAPA)], and *fac*-[Re(CO)$_3$(H**L^1**)Br], show higher concentration values of 0.357, 1.30, and 2.79 μg mg^{-1} protein, respectively. The highest levels of uptake are detected after treatment with *fac*-[Re(CO)$_3$(H**L^1**)Br], with a 119-fold increase in rhenium levels compared with cells treated with the rhenium standard, [Re(CO)$_5$(CF$_3$SO$_3$)] (Figure 10a).

The increased rhenium levels of *fac*-[Re(CO)$_3$(H**L^1**)Br] and *fac*-[Re(CO)$_3$(**L^1**)(DMAPA)] may be attributed to the increased lability of the monodentate ligating molecules, bromine and 3-dimethylamino-1-propylamine, in comparison to 4-picoline and pyridine. The lability of these ligands may facilitate coordination of the rhenium to intracellular or membrane proteins, consequently increasing the detection of rhenium in proportion to protein levels.

The [2 + 1] mixed-ligand complex *fac*-[Re(CO)$_3$(**L^1**)(4-picoline)] and the cationic tridentate species *fac*-[Re(CO)$_3$(**L^5**)]$^+$ were selected as appropriate candidates for further hypoxia studies as they demonstrated modest but not negligible uptake in nonhypoxic cells.

SH-(SY5Y) cells were cultivated to approximately 60% confluency, then transferred to a sealed GasPak EZ anaerobe container system with indicator and cultivated overnight to 80−90% confluency before treatment to induce hypoxia-like conditions. After the treatment solutions were prepared and

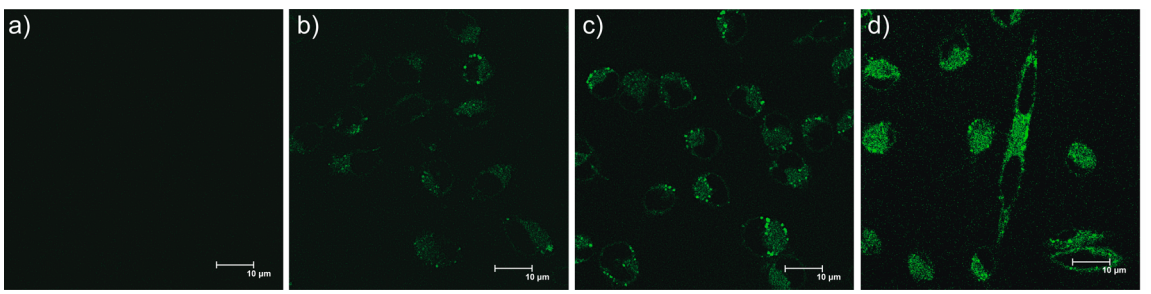

Figure 9. Confocal microscopy images of HeLa cells treated for 30 min at an excitation of λ 520 nm and with increasing concentrations of *fac*-[Re(CO)$_3$(**L^1**)(4-picoline)] in DMSO. (a) DMSO control (0 μM), (b) 10 μM, (c) 25 μM, and (d) 50 μM.

DOI: 10.1021/acs.inorgchem.5b01691
Inorg. Chem. XXXX, XXX, XXX−XXX

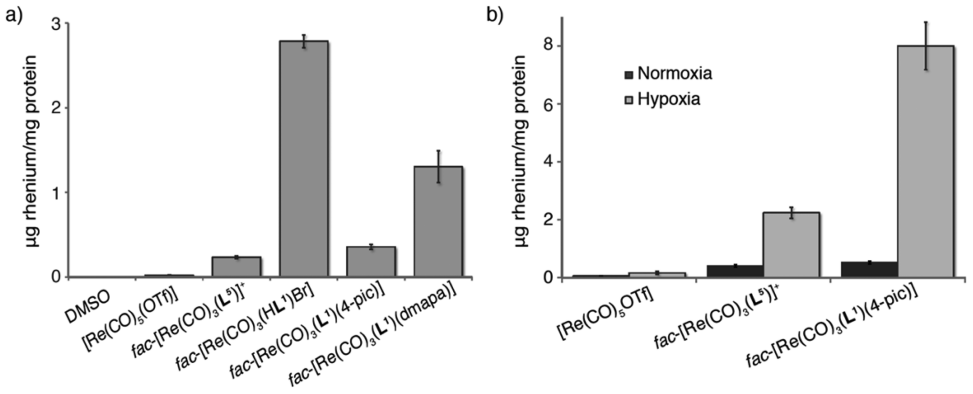

Figure 10. ICP-MS data of SH-(SY5Y) cells with rhenium complexes and control compounds. (a) Cells were subjected to normal oxygen levels and treated with compound (labeled). (b) Cells were subjected to both normoxic and hypoxic conditions (GasPak EZ aerobe container).

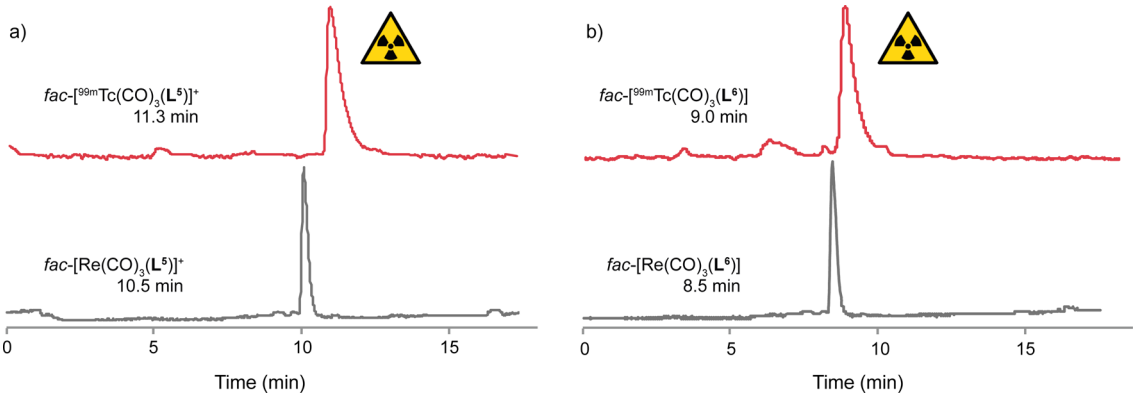

Figure 11. HPLC chromatograms (normalized) for (a) *fac*-$[Re(CO)_3(\mathbf{L}^5)]^+$ (below; UV detection, λ 254 nm) and radiolabeled *fac*-$[^{99m}Tc(CO)_3(\mathbf{L}^5)]^+$ (above; γ-ray detection) and (b) *fac*-$[Re(CO)_3(\mathbf{L}^6)]$ (below; UV detection, λ 254 nm) and radiolabeled *fac*-$[^{99m}Tc(CO)_3(\mathbf{L}^6)]$ (above; γ-ray detection).

media purged with N_2, the cells were again placed in the oxygen-deficient container with three GasPak EZ indicator sachets and incubated at 37 °C for 1 h.

The standard, $[Re(CO)_5(CF_3SO_3)]$, again shows minimal uptake into cells, while the tridentate *fac*-$[Re(CO)_3(\mathbf{L}^5)]^+$ demonstrates a 5.5-fold increase into hypoxia-induced cells with an initial rhenium concentration of 0.409 μg mg^{-1} protein compared to a concentration of 2.24 μg mg^{-1} protein in the hypoxia induced cells. Surprisingly, *fac*-$[Re(CO)_3(\mathbf{L}^1)$(4-picoline)] displays a 15.3-fold increase in cellular rhenium uptake for the hypoxic cells (0.524 vs 8.00 μg mg^{-1} protein; Figure 10b), indicating the bidentate nitrobenzene complexes, suggesting that the nitrobenzene complexes may be a viable alternative to conventional nitroimidazole-containing systems.

Techentium-99m Radiolabeling Experiments with HL^{1-2}, L^5 and HL^6/L^6Et. Radiolabeling was undertaken for all complexes and their retention times were compared to their rhenium analogues. The precursor *fac*-$[^{99m}Tc(CO)_3(H_2O)_3]^+$ (1000 MBq, 1 mL 0.9% saline solution) was formed using the commercially available lyophilized IsoLink kit. Slow oxidation of neutralized *fac*-$[^{99m}Tc(CO)_3(H_2O)_3]^+$ to $[^{99m}TcO_4]^-$ over the duration of experimentation (4−8 h) has been previously noted.[46]

Preparation of [2 + 1] mixed-ligand complexes involved reaction of the bidentate ligands HL^1 or HL^2 to the technetium-99m precursor at neutral pH with heating. The apical monodentate ligand (pyridine or 4-picoline) was added in excess as a 0.1 M aqueous solution (20−30 μL) and heated for a further 30 min. The extent of complexation was analyzed by RP-HPLC equipped with a UV and γ-ray detector with coinjection of cold rhenium analogues as reference compounds. Initial attempts at translating [2 + 1] rhenium chemistry to radioactive technetium-99m at the tracer level were marginally successful. The 4-nitro complex *fac*-$[^{99m}Tc(CO)_3(\mathbf{L}^1)$(4-picoline)] shows promise; however at least two radioactive species of similar concentrations are detected in the HPLC chromatogram of this complex, and further method development is required.

Ligands $\mathbf{L}^5$ and either $H\mathbf{L}^6$ or $\mathbf{L}^6$Et were separately mixed with aliquots of *fac*-$[^{99m}Tc(CO)_3(H_2O)_3]^+$ neutralized with 1.0 M HCl in a sealed vial, briefly sonicated, and heated at 65 °C for 35 min. Preparation of the complexes *fac*-$[^{99m}Tc(CO)_3(\mathbf{L}^5)]^+$ and *fac*-$[^{99m}Tc(CO)_3(\mathbf{L}^6)]$ resulted in radiochemical yields of above 90% (Figure 11). The cationic complex *fac*-$[^{99m}Tc(CO)_3(\mathbf{L}^5)]^+$ could be prepared with higher radiochemical purity than neutral *fac*-$[^{99m}Tc(CO)_3(\mathbf{L}^6)]$. The slight difference between retention times between the ^{99m}Tc-labeled compounds and their rhenium counterparts can, at least in part, be attributed to the sequential configuration of the UV and γ-ray detectors.

Evaluation of ^{99m}Tc-Labeled Tridentate Complex, *fac*-$[^{99m}Tc(CO)_3(\mathbf{L}^5)]^+$. The stability of the radiolabeled complex *fac*-$[^{99m}Tc(CO)_3(\mathbf{L}^5)]^+$ was tested by challenge reactions in 0.1 M phosphate buffered saline (PBS) and human plasma at 37 °C and analyzed by RP-HPLC at varying time intervals. Plasma stability studies for *fac*-$[^{99m}Tc(CO)_3(\mathbf{L}^5)]^+$ involved the

DOI: 10.1021/acs.inorgchem.5b01691
Inorg. Chem. XXXX, XXX, XXX−XXX

addition of the labeled complex in a PBS/HCl solution (0.15 mL, pH 7) to fresh human plasma from a healthy male. The plasma was incubated at 37 °C, and 0.1 mL aliquots were withdrawn after 10 min and 1, 2, and 4 h time intervals. No radioactive degradation products are detected over this time period for the radiolabeled complex.

The relative lipophilicity of the complex was determined by the addition of 10 μL of *fac*-$[^{99m}Tc(CO)_3(\mathbf{L}^5)]^+$ solution (approximately 10 MBq) to equal volumes of octanol and 0.1 M PBS, which was then shaken and separated. The radioactivity of each phase was measured and the partition coefficient (P) calculated (P = 0.52, cpm in octanol/cpm in PBS). The corresponding log $P_{(o/pbs)}$ value of −0.28 ± 0.03 indicates the hydrophilic nature of the tridentate cation.

Preliminary SPECT imaging studies of hypoxic tumors were undertaken in order to evaluate the feasibility of *fac*-$[^{99m}Tc(CO)_3(\mathbf{L}^5)]^+$ for future hypoxia imaging. Radiochemical purity was greater than 90% for all imaging studies.

Three BALB/c nude mice bearing human renal cell carcinoma (RCC; SK-RC-52) tumors were placed in supine and injected through the tail vein with approximately 20 MBq of *fac*-$[^{99m}Tc(CO)_3(\mathbf{L}^5)]^+$, and static images were acquired 2 h post injection. It has been established that intratumoral hypoxia exists within this cell line.[47] Each mouse had different tumor volumes: 400, 600, and 1100 mm^3 for mouse 1, 2, and 3, respectively. Tumor uptake is not evident for the 400 mm^3 (Mouse 1) or 1100 mm^3 (Mouse 3) tumor models. Significant tumor accumulation is visualized for the animal with a tumor volume of 600 mm^3, with a maximum standardized uptake value (SUV_{max}) of 6.4 and approximately 1.44%ID/g tissue on the basis of SPECT quantification (Figure 12). It is possible

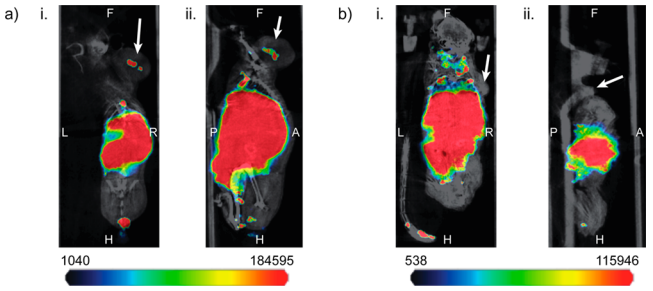

Figure 12. SPECT-CT images of *fac*-$[^{99m}Tc(CO)_3(\mathbf{L}^5)]^+$, 2 h p.i. (a) Mouse 2 (600 mm^3); (i) coronal projection, (ii) sagittal plane. (b) Mouse 1 (400 mm^3); (i) coronal projection, (ii) sagittal plane. Arrows indicate tumor site. Scale bar indicates number of counts per voxel.

that the small tumor in Mouse 1 was too small for significant hypoxia, but this was not verified. A separate PET/CT study of the Mouse 3 (1100 mm^3) with the hypoxia tracer ^{18}F-FMISO also revealed little penetration of the tracer into the tumor but a small amount of uptake of the tracer around the outer edge of the necrotic core (Figure 13). The SK-RC-52 tumor model has been well characterized, and tumor size does serve as a useful guide to tumor hypoxia, but it is acknowledged that hypoxia cannot be predicted by tumor size alone.[47−49] The promising results from this pilot study suggest that *fac*-$[^{99m}Tc(CO)_3(\mathbf{L}^5)]^+$ warrants further attention in more detailed studies that include parallel oxygen determination measurements.

CONCLUDING REMARKS

A series of ligands ($H\mathbf{L}^{1-4}$) and their matching, neutral rhenium complexes *fac*-$[Re(CO)_3(H\mathbf{L}^{1-4})(Br)]$ and *fac*-$[Re(CO)_3(\mathbf{L}^{1-4})(X)]$ (X = 4-picoline, pyridine, DMAPA) were synthesized by microwave-assisted thermal heating with short reaction times to give products in good yields and high purity. These complexes were characterized by mass spectroscopy, NMR, IR, UV−visible and fluorescence spectroscopy, and X-ray crystallography. Electrochemical studies investigated the relative inductive influences and resonance effects of the assorted ligand substituents (H, OCH_3, *m*-NO_2, *p*-NO_2), in addition to highlighting the complicated mechanism of reduction of the nitrobenzene-containing species. Cyclic voltammetry reveals reductive processes for the nitro-bearing rhenium complexes with $E^{0\prime}$ values between −0.6 and −1.1 V that are within biologically accessible electrochemical potentials. Crystallographic studies show that ligands $H\mathbf{L}^{1-2}$ crystallize as their *E* isomer around the C═N bond. Crystal structures of complexes with apical bromo-ligand substitution, *fac*-$[Re(CO)_3(H\mathbf{L}^{1-4})(Br)]$, confirm the assumptions based on NMR data, suggesting that the bidentate hydrazine ligand remains protonated at the hydrazinic N*H* following coordination. Upon exchange of the apical, monodentate ligand with *N*-heterocyclic compounds, pyridine or picoline, the hydrazinic nitrogen atom is deprotonated, inducing interesting visible spectroscopic changes.

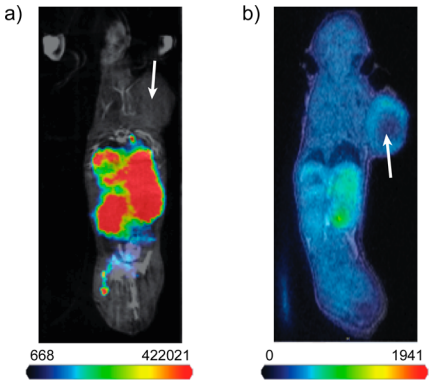

Figure 13. (a) SPECT/CT image of Mouse 3 (1100 mm^3) injected with *fac*-$[^{99m}Tc(CO)_3(\mathbf{L}^5)]^+$, coronal projection showing no tumor uptake. (b) PET/MR of Mouse 3 injected with ^{18}F-FMISO, coronal projection showing tumor necrosis and a hypoxic rim around the central necrotic core. Administration and scanning of ^{18}F-FMISO accumulation occurred 2 h post tracer injection. Arrows indicate tumor site, and the scale bar indicates number of counts per voxel.

Two tridentate ligands bearing a nitroimidazole functional group, $\mathbf{L}^5$ and $H\mathbf{L}^6$, were synthesized and used to prepare cationic *fac*-$[Re(CO)_3(\mathbf{L}^5)]^+$ and neutral *fac*-$[Re(CO)_3(\mathbf{L}^6)]$. Crystallographic analysis of *fac*-$[M(CO)_3(\mathbf{L}^5)]^+$ shows a predictable six-coordinate distorted octahedral geometry with a *N,N,N* ligand binding mode upon complexation. Electrochemical analysis using cyclic voltammetry indicates reduction of the nitro group in the cathodic region of interest for biological hypoxia detection for both *fac*-$[Re(CO)_3(\mathbf{L}^5)]^+$ and *fac*-$[Re(CO)_3(\mathbf{L}^6)]$.

The cellular uptake and retention of the [2 + 1] complex *fac*-$[Re(CO)_3(\mathbf{L}^1)(4\text{-picoline})]$ and the cationic complex prepared with the neutral tridentate ligand *fac*-$[Re(CO)_3(\mathbf{L}^5)]^+$ was investigated in normoxic and hypoxic SH-(SY5Y) cells. The cationic complex *fac*-$[Re(CO)_3(\mathbf{L}^5)]^+$ has a 5-fold increase in retention in hypoxia-induced cells, and *fac*-$[Re(CO)_3(\mathbf{L}^1)(4\text{-picoline})]$ displays a 15-fold increase in hypoxic cells.

Forming complexes with high radiochemical purity was more straightforward with the tridentate ligands, $\mathbf{L}^5$ and $H\mathbf{L}^6$, than

DOI: 10.1021/acs.inorgchem.5b01691
Inorg. Chem. XXXX, XXX, XXX−XXX

with the nitro-containing [2 + 1] mixed-ligand systems. Complex *fac*-$[^{99m}Tc(CO)_3(\mathbf{L}^5)]^+$ is stable in human serum and relatively hydrophilic, yet it is still cell permeable (log $P_{(o/pbs)} = -0.28$). Preliminary SPECT/CT imaging with *fac*-$[^{99m}Tc(CO)_3(\mathbf{L}^5)]^+$ in a well characterized model of tumor hypoxia revealed significant tumor accumulation ($SUV_{max} = 6.4$, 1.44%ID/g), and this complex warrants further investigation in more detailed hypoxia models. Ligands $\mathbf{L}^5$ and $\mathbf{L}^6$ also form stable complexes with the *fac*-$\{Re(CO)_3\}^+$ core, so investigations into radiolabeling with the therapeutic β-emitting $^{186/188}Re$ isotopes are warranted with a view to developing complexes suitable for both diagnostic imaging and therapy.

EXPERIMENTAL SECTION

General Procedures. All reagents and solvents, unless otherwise stated, were purchased from standard commercial sources and were used as received. Anhydrous ethanol (EtOH) was dried over magnesium ethoxide under a nitrogen environment. *N*,*N*-dimethylformamide (DMF) was distilled and dried over magnesium sulfate and stored over 4 Å molecular sieves. Acetonitrile (CH_3CN) was dried over K_2CO_3, distilled, and stored over 3 Å molecular sieves. All reactions were undertaken under inert conditions unless otherwise indicated. A Biotage Initiator Sixty EXP 2.0 Microwave Reactor was utilized for all microwave-assisted reactions. Thin-layer chromatography (TLC) was performed on Merck aluminum backed 2-μm-thick silica gel plates (60 GF_{254}) and were visualized under λ 254 nm UV light or stained with 20% *w*/*v* phosphomolybdic acid in ethanol, iodine dip, or 20% *w*/*v* copper chloride in acetone where relevant. Column chromatography was performed on silica gel (Kieselgel 60, 230−400 mesh) using the indicated solvent system. Nuclear Magnetic Resonance (NMR) spectra were acquired on a superconducting Varian-FT-NMR 500 spectrometer (Varian, California, USA). All NMR were acquired at 25 °C. ^1H and $^{13}C\{^1H\}$ chemical shifts were referenced to residual solvent peaks and are quoted in parts per million relative to TMS. Mass Spectra (MS) were recorded on an Agilent 6220 Q-TOF LC/MS (Agilent, California, USA) mass spectrometer and/or a Waters-Micromass QuattroII triple quadrupole electrospray ionization mass spectrometer. Cyclic voltammograms were recorded on an AUTOLAB PGSTAT100 electrochemical workstation using GPES V4.9 software. A glassy-carbon working electrode, platinum wire counter electrode, and Ag/Ag^+ (silver wire immersed in 0.01 M $AgNO_3/CH_3CN$) reference electrode were utilized for all measurements. Measurements were taken in deoxygenated, anhydrous CH_3CN with 0.1 M supporting electrolyte, $[NH_4][BF_4]$, and 1.0 mM analyte unless otherwise specified. Each solution was measured at ambient temperature, and the cell was kept under a N_2 atmosphere throughout the experiment. Cathodic peak potentials (E_{pc}) and half-wave potential ($E^{0\prime}$) were measured relative to an internal reference ferrocenium/ferrocene (Fc^+/Fc) redox couple, where $E^{0\prime}$ was designated as +400 mV vs a saturated calomel electrode (SCE) in acetonitrile.[31]

Analytical Reverse Phase High Performance Liquid Chromatography (RP-HPLC) was undertaken using an Agilent 1100 Series HPLC System using a Zorbax Eclipse XDB-C18 column (4.6 × 150 mm, 5 μm) at a flow rate of 1 mL min^{-1}. **System A**: Gradient elution of buffer A (0.1% TFA in H_2O) and buffer B (0.1% TFA in CH_3CN) from 0 to 100% B to A over 25 min and UV detection at λ 214, 254, and 280 nm. **System B**: Gradient elution of buffer A (0.1% TFA in H_2O) and buffer B (0.1% TFA in CH_3CN) from 0 to 40% B to A over 25 min and UV detection at λ 214, 254, and 280 nm.

UV−visible absorption spectra were recorded on a Shimadzu UV-1650PC UV−visible spectrophotometer using UVPC v3.9 software. Emission spectra were obtained on a Varian CARY Eclipse fluorescence spectrophotometer. Both absorption and emission spectra measurements were performed in capped quartz cuvettes in THF or CH_3CN.

Infrared spectra (IR) were recorded neat on a PerkinElmer Spectrum One FT-IR spectrometer with a zinc selenide/diamond universal ATR 60 sampling accessory, as a thin film using cm^{-1} as units of measurement. Melting points were determined using an EZ-Melt MPA 120 Automated Melting Point Apparatus from Stanford Research Systems and are uncorrected.

Analytical radio-HPLC was performed using a Shimadzu 10 AVP UV−visible spectrophotometer (Shimadzu, Kyoto, Japan) with two LC-10ATVP solvent delivery systems for solvents A and B. Peak separation was achieved using a Nacalai Tesque Cosomosil 5C18-AR Waters column (4.6 × 150 mm, 5 μm; Nacalai Tesque, Kyoto, Japan) at 1 mL min^{-1}. **System C**: Gradient elution of buffer A (0.1% TFA in H_2O) and buffer B (0.1% TFA in CH_3CN) from 0 to 100% B to A, over 20 min and UV detection at λ 254 nm.

Human blood samples were centrifuged with a Heraeus Labofuge 6000 centrifuge at 3000*g* for 10 min (Heraeus, Hanau, Germany). Radioactivity readings for serum stability studies were taken with a Capintec CRC-35R dose calibrator (Capintec, New Jersey, USA) and were measured in MBq.

Centrifugation of radioactive compounds was undertaken using an Eppendorf 5415 D centrifuge (Eppendorf, Hamburg, Germany). Partition coefficient data were collected with a PerkinElmer, Wizard 1470 (PerkinElmer, Massachusetts, USA) automatic γ counter, which measured the radioactive decay of each sample in counts per minute (cpm).

SPECT images were obtained using a Mediso nanoScan SPECT/CT (and MRI subsystem; Mediso Medical Imaging Systems, Budapest, Hungary) equipped with a multipinhole (M^3) collimator. Visualization and evaluation of SPECT data was carried out using PMOD fusion software (PMOD technologies, Switzerland). Organ uptake was initially expressed as counts per voxel and then calculated as the percentage of injected dose (%ID) and percentage of injected dose per gram (%ID/g) volume. Animals were imaged at the Australian Cancer Research Foundation (ACRF) Centre for Translational Cancer Therapeutics and Imaging.

Syntheses. $[Re(CO)_5OTf]$,[50] 1*H*-imidazol-2-amine sulfate,[51] potassium 2-nitro-1*H*-imidazolide,[37] 1-(3-bromopropyl)-2-nitro-1*H*-imidazole,[37] and *N*-(2-pyridylmethyl)aminoethyl acetate[52] were synthesized according to previously reported procedures. Ligands HL^1 and HL^2 are known compounds and their spectroscopic details are available from the literature;[53,54] however NMR spectral data and melting points vary significantly from values obtained for this research, therefore full spectral analysis has been provided.

***HL*^{1}.** To 2-hydrazinopyridine (3.00 g, 27 mmol) in ethanol (40 mL) was added 4-nitrobenzaldehyde (4.15 g, 27 mmol). The resulting suspension was stirred for 4 h at RT. The precipitate was collected via vacuum filtration and washed with cold ethanol (3 × 10 mL) and diethyl ether (3 × 10 mL). The solid was purified by column chromatography (CH_2Cl_2/CH_3OH, 95:5), and the desired fractions were recrystallized from hot dichloromethane to give orange stick needles (5.02 g, 77%). ^1H NMR [DMSO-d_6, 400 MHz]: δ (ppm) 11.3 (1H, s, N*H*), 8.23 (2H, AA′XX′, Ar*H*), 8.16 (1H, d, J = 4.4 Hz, py*H*), 8.09 (1H, s, C*H*═N), 7.90 (2H, AA′XX′, Ar*H*), 7.69 (1H, t, J = 7.6 Hz, py*H*), 7.32 (1H, d, J = 8.4 Hz, py*H*) 6.84 (1H, t, J = 6.0 Hz, py*H*). $^{13}C\{^1H\}$ NMR [DMSO-d_6, 125.7 MHz]: δ (ppm) 156.5 (C, pyC), 147.9 (C, ArC-NO_2), 146.5 (C, pyC), 142.0 (C, CH═N), 138.1 (C, ArC), 136.0 (C, pyCH), 126.5 (2C, ArCH), 124.0 (2C, ArCH), 115.9 (C, pyCH), 106.8 (C, pyCH). IR: ν (cm^{-1}) 2987 (Ar C−H), 1504 ($ArNO_2$, $\nu_{as}(N{=}O)_2$) 1333 ($ArNO_2$, $\nu_{sym}(N{=}O)_2$). HRMS (ESI^+) m/z calcd for $C_{12}H_{11}N_4O_2$: 243.0882. Found: 243.0877 {$[M + H]^+$, 100%}. mp: 231−237 °C. Crystals suitable for single crystal X-ray crystallography were grown from a concentrated solution in dimethysulfoxide.

***HL*^{2}.** The procedure is as that for HL^1, except using 2-hydrazinopyridine (3.00 g, 27 mmol), ethanol (40 mL), and 3-nitrobenzaldehyde (4.15 g, 27 mmol). The solid was recrystallized from hot chloroform to afford a yellow fluffy solid (4.81 g, 74%). ^1H NMR [CH_3CN-d_3, 500 MHz]: δ (ppm) 10.4 (1H, s, N*H*), 8.47 (1H, s, Ar*H*), 8.13−8.10 (2H, m, Ar*H*), 8.07 (1H, s, C*H*═N), 8.04 (1H, dtd, J = 7.8, 1.3, 0.5 Hz, py*H*), 7.65 (1H, ddd, J = 8.4, 1.2, 1.9 Hz, py*H*), 7.61 (1H, t, J = 8.0 Hz, Ar*H*), 7.33 (1H, dt, J = 8.4, 1.0 Hz, py*H*), 6.80 (1H, ddd, J = 7.2, 4.9, 1.0 Hz, py*H*). $^{13}C\{^1H\}$ NMR [DMSO-d_6, 125.7 MHz]: δ (ppm) 156.7 (C, pyC), 148.3 (C, ArC-NO_2), 147.8 (C,

DOI: 10.1021/acs.inorgchem.5b01691
Inorg. Chem. XXXX, XXX, XXX−XXX

pyCH), 138.1 (C, N=CH), 137.3 (C, ArC), 136.2 (C, pyC), 132.0 (C, ArCH), 130.3 (C, ArCH), 122.6 (C, ArCH), 119.8 (C, ArCH), 115.6 (C, pyCH), 106.6 (C, pyCH). IR: ν (cm^{-1}) 2972−2901 (Ar C−H), 1520 ($ArNO_2$, $\nu_{as}(N{=}O)_2$), 1343 ($ArNO_2$, $\nu_{sym}(N{=}O)_2$). HRMS (ESI^+) m/z calcd for $C_{12}H_{11}N_4O_2$: 243.0882. Found: 243.0877 {$[M + H]^+$, 100%}; mp 220−228 °C. Crystals suitable for single crystal X-ray crystallography were grown from a concentrated solution in dimethyl sulfoxide.

HL³ (+ 1/4 H_2O). The procedure is as that for HL^1, except using 2-hydrazinopyridine (0.81 g, 7.4 mmol), ethanol (10 mL), and 4-methoxybenzaldehyde (0.89 mL, 7.4 mmol). The collected precipitate was sufficiently clean to proceed without further purification and was obtained as a white fluffy solid (1.20 g, 72%). ^1H NMR [DMSO-d_6, 500 MHz]: δ (ppm) 10.7 (1H, s, NH), 8.08 (1H, ddd, J = 4.9, 1.9, 0.9 Hz, pyH), 7.98 (1H, s, CH=N), 7.63−7.59 (3H, m, pyH, ArH, ArH), 7.21 (1H, dt, J = 8.4, 0.9 Hz, pyH), 6.97 (2H, AA′XX′, ArH), 6.72 (1H, ddd, J = 7.1, 4.9, 1.0 Hz, pyH), 3.78 (3H, s, CH_3). $^{13}C\{^1H\}$ NMR [DMSO-d_6, 125.7 MHz]: δ (ppm) 159.7, 157.2, 147.7, 138.8, 137.8, 128.1 (2C, ArCH), 127.3 (C, ArC), 114.5 (C, pyCH), 114.2 (2C, ArCH), 106.1 (C, pyCH), 55.2 (C, OCH_3). IR: ν (cm^{-1}) 3180−2836 (Ar/py C−H), 1596 (C=C, C=N), 1438 (C=C, C=N), 1244 (OCH_3, ν_{as}(C−O−C)), 1036 (OMe, ν_{sym}(C−O−C)). HRMS (ESI^+) m/z calcd for $C_{13}H_{14}N_3O$: 227.11369. Found: 227.1141 {$[M + H]^+$, 100%}. mp: 165−167 °C.

HL⁴ (+ 1/4 H_2O). The procedure is as that for HL^1, except using 2-hydrazinopyridine (0.80 g, 7.1 mmol), ethanol (10 mL), and benzaldehyde (0.82 mL, 7.1 mmol). The collected precipitate was sufficiently clean to proceed without further purification and was obtained as a pale yellow solid (1.0 g, 72%). ^1H NMR [$CDCl_3$, 500 MHz]: δ (ppm) 10.9 (1H, s, NH), 8.11 (1H, ddd, J = 4.9, 1.9, 0.9 Hz, pyH), 8.03 (1H, s, CH=N), 7.67−7.62 (3H, m, ArH, ArH, pyH), 7.40 (2H, dd, J = 8.0, 6.9 Hz, ArH), 7.32 (1H, tt, J = 7.0, 1.5 Hz), 7.25 (1H, dt, J = 8.4, 0.9 Hz), 6.79 (1H, ddd, J = 7.1, 4.9, 1.0 Hz, pyH). $^{13}C\{^1H\}$ NMR [$CDCl_3$, 125.7 MHz]: δ (ppm) 156.7, 147.0, 139.7, 138.6, 135.0, 129.0 (2C, ArCH), 126.6 (2C, ArCH), 115.8 (C, pyCH), 107.9 (C, pyCH). IR: ν (cm^{-1}) 3195−2901 (Ar/py C−H), 1603 (C=C, C=N), 1436 (C=C, C=N). HRMS (ESI^+) m/z calcd for $C_{12}H_{11}N_4O_2$: 198.1031. Found: 198.1032 {$[M + H]^+$, 100%}. mp: 150−152 °C.

fac-[Re(H_2O)$_3$(CO)$_3$]Br. This compound was prepared by a modification of a previously reported procedure.[55] To bromopentacarbonyl rhenium(I) (0.40 g, 0.98 mmol) was added degassed Milli-Q water (10 mL). The suspension was subjected to microwave heating for 10 min at 150 °C. The reaction mixture was vigorously shaken then resubjected under the same conditions (×2). The solution was filtered hot and reduced *in vacuo* to afford a pale green powder (0.39 g, 98%). IR: ν (cm^{-1}) 2018 (*fac*-ν(C≡O)), 1910 (*fac*-ν(C≡O)).

fac-[Re(H_2O)$_3$(CO)$_3$]OTf. This compound was prepared by a modification of a previously reported procedure.[55,56] To pentacarbonyl(trifluoromethanesulfonato) rhenium(I) (0.30 g, 0.63 mmol) was added degassed Milli-Q water (6.3 mL). The suspension was subjected to microwave heating for 15 min at 155 °C. The reaction mixture was stored as a 0.1 M solution (approx.) in water.

fac-[Re(CO)$_3$(pyridine)$_3$]OTf. This compound was prepared by a modification of a previously reported procedure.[56] To pentacarbonyl-(trifluoromethanesulfonato) rhenium(I) (0.19 g, 0.31 mmol) purged with N_2 was added degassed pyridine (4 mL). The solution was subjected to microwave conditions at 150 °C for 15 min. The pyridine was reduced to approximately 1/4 under a high vacuum and diethyl ether (4 mL) added and stirred vigorously, whereby a white solid precipitated. The solid was filtered and washed with copious amounts of cold diethyl ether to afford white crystals (0.22 g, 83%). ^1H NMR [CH_3CN-d_3, 500 MHz]: δ (ppm) 8.51 (6H, d, J = 6.0 Hz, pyH), 8.10 (3H, t, J = 7.5 Hz, pyH), 7.54 (6H, t, J = 7.0 Hz, pyH). $^{13}C\{^1H\}$ NMR [CH_3CN-d_3, 125.7 MHz]: δ (ppm) 154.7 (6C, ArCH), 141.4 (6C, ArCH), 128.1 (3C, ArCH). IR: ν (cm^{-1}) 2027 (*fac*-ν(C≡O)), 1908 (*fac*-ν(C≡O)). HRMS (ESI^+) m/z calcd for $C_{18}H_{15}N_3O_3Re$: 508.0671. Found: 508.0680 {[M-OTf]$^+$, 100%}. RP-HPLC (System A): R_T (min) 11.9.

fac-[Re(CO)$_3$(4-picoline)$_3$]OTf. This compound was prepared by a modification of a previously reported procedure.[56] Freshly distilled 4-picoline (2 mL) was added to pentacarbonyl-(trifluoromethanesulfonato) rhenium(I) (0.16 g, 0.33 mmol) and subjected to microwave conditions at 150 °C for 15 min (×2). The solution was cooled to RT, and diethyl ether (6 mL) was added. The resulting precipitate was filtered and washed with cold diethyl ether to afford a white powder (0.18 g, 78%). ^1H NMR [CH_3CN-d_3, 500 MHz]: δ (ppm) 8.31 (6H, AA′XX′, picH), 7.36 (6H, AA′XX′, picH), 2.44 (9H, s, CH_3). $^{13}C\{^1H\}$ NMR [CH_3CN-d_3, 125.7 MHz]: δ (ppm) 154.1 (3C, ArC), 153.9 (6C, ArCH), 128.7 (6C, ArCH), 21.30 (9C, CH_3). IR: ν (cm^{-1}) 2027 (*fac*-ν(C≡O)), 1903 (*fac*-ν(C≡O)). HRMS (ESI^+) m/z calcd for $C_{21}H_{21}N_3O_3Re$: 550.1140. Found: 550.1142 {[M-OTf]$^+$, 100%}. RP-HPLC (System A): R_T (min) 14.0

fac-[Re(CO)$_3$(DMAPA)$_3$]2OTf. This compound was prepared by a modification of a previously reported procedure[56] but was not isolated; formation was determined by ESI-MS. ESI-MS calcd for $C_{18}H_{42}N_6O_3Re$ m/z 577.2876. Found: 577.2888 {[M-2OTf]$^+$, 100%}

fac-[Re(CO)$_3$(HL^1)Br]. Rhenium triaquatricarbonyl bromide (0.1 g, 0.25 mmol) was stirred in anhydrous methanol (10 mL). HL^1(0.06 g, 0.25 mmol) was added to the solution under an inert atmosphere and stirred at RT for 4 h. The resulting precipitate was collected via vacuum filtration and washed with cold methanol. A yellow solid was obtained as *fac*-[Re(CO)$_3$(HL^1)Br] (0.09 g, 60%) which turned a deep pink/purple in solution. ^1H NMR [DMSO-d_6, 500 MHz]: δ (ppm) 13.2 (1H, br s, NH), 8.67 (1H, s, CH=N), 8.42 (2H, AA′XX′, ArH), 8.36 (1H, d, J = 5.2 Hz, pyH), 7.99 (2H, AA′XX′, ArH), 7.91 (1H, tdd, J = 7.5, 7.0, 1.5 Hz, pyH), 7.12 (1H, d, J = 8.5 Hz, pyH), 6.98 (1H, t, J = 6.5 Hz, pyH). $^{13}C\{^1H\}$ NMR [DMSO-d_6, 125.7 MHz]: δ (ppm) 196.6 (C, CO), 196.5 (C, CO), 194.6 (C, CO), 155.1 (C, pyCH), 151.3, 149.5, 148.3 (C, ArC-NO_2), 140.8, 140.2, 131.0 (2C, ArCH), 123.6 (2C, ArCH), 117.2 (C, pyCH), 108.2 (C, pyCH). IR: ν (cm^{-1}) 2988 (Ar C−H, N−H), 2022 (*fac*-ν(C≡O)), 1894 (*fac*-ν(C≡O)), 1522 ($ArNO_2$, $\nu_{as}(N{=}O)_2$) 1357 ($ArNO_2$, $\nu_{sym}(N{=}O)_2$). HRMS (ESI^-) m/z calcd for $C_{15}H_9BrN_4O_5Re$: 590.9314. Found: 590.9314 {$[M-H]^-$, 100%}. RP-HPLC (System A): R_T (min) 15.31. Crystals suitable for single crystal X-ray crystallography were grown from slow evaporation of a concentrated solution in acetonitrile.

fac-[Re(CO)$_3$(HL^2)Br]. This procedure is as per that for *fac*-[Re(CO)$_3$(HL^1)Br] except using HL^2 as the ligand. A pale yellow powder was obtained as *fac*-[Re(CO)$_3$(HL^2)Br] (0.12 g, 80%). ^1H NMR [DMSO-d_6, 500 MHz]: δ (ppm) 13.2 (1H, s, NH), 8.71 (1H, s, ArH), 8.66 (1H, s, CH=N), 8.41 (1H, d, J = 8 Hz, ArH), 8.36 (1H, d, J = 4.5 Hz, ArH), 8.17 (1H, d, J = 7.5 Hz, pyH), 7.88 (2H, m, ArH, pyH), 7.11 (1H, d, J = 8.5 Hz, pyH), 6.97 (1H, t, J = 5.5 Hz, pyH). $^{13}C\{^1H\}$ NMR [DMSO-d_6, 125.7 MHz]: δ (ppm) 196.1 (C, CO) 194.8 (C, CO), 190.5 (C, CO), 155.2 (C, pyC), 150.9 (C, N=CH), 149.4 (C, pyCH), 147.5 (C, C-NO_2), 140.7, 135.9, 135.3 (C, ArC), 130.3, 125.0, 124.6 (C, ArCH), 117.1 (C, pyCH), 108.1 (C, pyCH). IR: ν (cm^{-1}) 3184−3051 (ν(N−H)), 2023 (*fac*-ν(C≡O)), 1902 (*fac*-ν(C≡O)), 1519 ($ArNO_2$, $\nu_{as}(N{=}O)_2$), 1344 ($ArNO_2$, $\nu_{sym}(N{=}O)_2$). HRMS (ESI^+) m/z calcd for $C_{15}H_{10}N_4O_5Re$: 513.0203. Found: 513.0203 {$[M-Br]^+$, 100%}. RP-HPLC (System A): R_T (min) 14.2. Crystals suitable for single crystal X-ray crystallography were grown from slow evaporation of a concentrated solution in acetonitrile.

fac-[Re(CO)$_3$(HL^3)Br]. This procedure is as per that for *fac*-[Re(CO)$_3$(HL^1)Br] except using HL^3 (0.06 g, 0.25 mmol) as the ligand. An off-white powder was obtained as *fac*-[Re(CO)$_3$(HL^3)Br] (0.07 g, 49%). ^1H NMR [DMSO-d_6, 500 MHz]: δ (ppm) 12.8 (1H, br s, NH), 8.52 (1H, s, CH=N), 8.34 (1H, ddd, J = 5.9, 1.6, 0.8 Hz, pyH), 7.86 (1H, t, J = 7.0 Hz, pyH), 7.81 (2H, AA′XX′, ArH), 7.12 (2H, AA′XX′, ArH), 7.05 (1H, dt, J = 8.5, 0.9 Hz, pyH), 6.92 (1H, ddd, J = 7.2, 5.9, 1.2 Hz pyH). $^{13}C\{^1H\}$ NMR [DMSO-d_6, 125.7 MHz]: δ (ppm) 196.4 (C, CO), 194.9 (C, CO), 191.3 (C, CO), 161.5 (C, ArC-OCH_3), 155.4 (C, pyC), 153.4 (C, N=CH), 149.3 (C, pyCH), 140.3 (C, pyCH), 131.7 (2C, ArCH), 125.6 (C, ArC), 116.4 (C, pyCH), 114.0 (2C, ArCH), 107.9 (C, pyCH), 55.5 (C, OCH_3). IR: ν (cm^{-1}) 3182−2931 (ν(N−H)), 2020 (*fac*-ν(C≡O)), 1916 (*fac*-ν(C≡O)1878 (*fac*-ν(C≡O)), 1605 (C=C, C=N), 1484 (C=C, C=N), 1263 (OCH_3, ν_{as}(C−O−C)), 1176 (OCH_3, ν_{sym}(C−O−C)).

DOI: 10.1021/acs.inorgchem.5b01691
Inorg. Chem. XXXX, XXX, XXX−XXX

HRMS (ESI$^+$) m/z calcd for $C_{16}H_{13}N_3O_4Re$: 498.0464. Found: 498.0470 {[M−Br]$^+$, 100%}. RP-HPLC (System A): R_T (min) 15.0. Crystals suitable for single crystal X-ray crystallography were grown from slow evaporation of a concentrated solution in acetonitrile.

fac-[Re(CO)$_3$(HL^4)Br]. This procedure is as per that for *fac*-[Re(CO)$_3$(HL^1)Br] except using HL^4 (0.05 g, 0.25 mmol) as the ligand. A pale yellow powder was afforded as *fac*-[Re(CO)$_3$(HL^4)Br] (0.09 g, 69%). ^{1}H NMR [DMSO-d_6, 500 MHz]: δ (ppm) 12.9 (1H, br s, N*H*), 8.61 (1H, s, C*H*═N), 8.34 (1H, ddd, J = 5.8, 1.6, 0.8 Hz, py*H*), 7.88 (1H, ddd, J = 8.6, 7.2, 1.5 Hz, py*H*), 7.77−7.75 (2H, m, Ar*H*), 7.56−7.55 (3H, m, Ar*H*), 7.07 (1H, dt, J = 8.5, 1.0 Hz, py*H*), 6.94 (1H, ddd, J = 7.2, 5.9. 1.2, py*H*). ^{13}C{^{1}H} NMR [DMSO-d_6, 125.7 MHz]: δ (ppm) 196.4 (C, *C*O) 194.4 (C, *C*O), 191.1 (C, *C*O), 155.3 (C, py*C*), 153.3 (C, N═*C*H), 149.4 (C, py*C*H), 140.4, 133.6 (C, Ar*C*), 130.7, 129.4 (2C, Ar*C*H), 128.5 (2C, Ar*C*H), 116.6 (C, py*C*H), 107.9 (C, py*C*H). IR: ν (cm^{-1}) 3180−3020 (ν(N−H)), 2020 (*fac*-ν(C≡O)), 1921 (*fac*-ν(C≡O)), 1885 (*fac*-ν(C≡O)), 1626−1427 (py C−N, C−C). HRMS (ESI$^+$) m/z calcd for $C_{15}H_{11}N_3O_3Re$: 468.0358. Found: 468.0440 {[M-Br]$^+$, 100%}. RP-HPLC (System A): R_T (min) 15.2. Crystals suitable for single crystal X-ray crystallography were grown from slow evaporation of a concentrated solution in acetonitrile.

fac-[Re(CO)$_3$(L^1)(4-picoline)]. Degassed, anhydrous CH_3OH (2 mL) was added to HL^1 (0.04 g, 0.14 mmol). The *tris*-substituted rhenium complex *fac*-[Re(CO)$_3$(4-picoline)$_3$]OTf (0.1 g, 0.14 mmol) was dissolved in degassed, anhydrous CH_3OH (3 mL) and added to the suspension. The reaction mixture was subjected to microwave irradiation at 155 °C for 2 × 10 min. The solution was cooled, and the resultant precipitate was collected via vacuum filtration. The filtrate was collected and reduced *in vacuo* to approximately 1/2 the initial volume, followed by the addition of Et_2O to yield a second crop of the desired product. A forest-green, crystalline solid was obtained (0.07 g, 80%). ^{1}H NMR [CH_3CN-d_3, 500 MHz]: δ (ppm) 8.65 (2H, AA′XX′, Ar*H*), 8.35 (1H, dd, J = 6.0, 0.6 Hz, py*H*), 8.32 (2H, d, J = 5.5 Hz, pic*H*), 8.21 (2H, AA′XX′, Ar*H*), 7.87 (1H, s, Ar*H*), 7.45−7.42 (1H, t, J = 8.0 Hz, py*H*), 7.17 (2H, dd, J = 5.9, 0.4 Hz, pic*H*), 6.90 (1H, d, J = 8.7 Hz, py*H*), 6.42 (1H, t, J = 6.4 Hz, py*H*), 2.30 (3H, s, C*H*$_3$). ^{13}C{^{1}H} NMR [CH_3CN-d_3, 125.7 MHz]: δ (ppm) 199.0 (C, *C*O) 198.9 (C, *C*O), 195.7 (C, *C*O), 170.5 (C, py*C*), 153.1 (C, pic*C*$_{an}$), 152.2 (2C, pic*C*H$_{an}$), 149.2 (C, py*C*H), 147.2 (C, *C*-NO$_2$), 141.5 (C, N═*C*H), 140.5 (C, Ar*C*), 139.3 (C, Ar*C*H), 132.2 (2C, Ar*C*H), 128.0 (2C, pic*C*H$_{an}$), 124.3 (2C, Ar*C*H), 114.9 (C, py*C*H), 113.3 (C, py*C*H), 21.11 (C, pic*C*H$_3$). IR: ν (cm^{-1}) 2016 (*fac*-ν(C≡O)), 1929 (*fac*-ν(C≡O)), 1897 (*fac*-ν(C≡O)), 1505 (ArNO$_2$, ν_{as}(N═O)$_2$) 1332 (ArNO$_2$, ν_{sym}(N═O)$_2$). HRMS (ESI$^+$) m/z calcd for $C_{21}H_{17}N_5O_5Re$: 606.0787. Found: 606.0805 {[M + H]$^+$, 100%}. RP-HPLC (System A): R_T (min) 14.2. Crystals suitable for single-crystal X-ray crystallography were grown from slow evaporation of a concentrated solution of the product in acetonitrile.

fac-[Re(CO)$_3$(L^2)(4-picoline)]. This procedure is as that for *fac*-[Re(CO)$_3$(4-picoline)$_3$L^1], except using HL^2 (0.04 g, 0.14 mmol), *fac*-[Re(CO)$_3$(4-picoline)$_3$]OTf (0.10 g, 0.14 mmol), and CH_3OH (4 mL). Bright orange crystals were obtained from the reaction mixture (0.06 g, 69%). ^{1}H NMR [CH_3CN-d_3, 500 MHz]: δ (ppm) 9.66 (1H, s, C*H*═N), 8.58 (1H, d, J = 7.9 Hz, Ar*H*), 8.34−8.30 (3H, m, pic*H*, py*H*), 8.13 (1H, d, J = 7.7 Hz, Ar*H*), 7.89 (1H, s, Ar*H*), 7.62 (1H, td, J = 8.1, 1.5 Hz, Ar*H*), 7.39 (1H, ddt, J = 8.7, 6.9, 1.8 Hz, py*H*), 7.17 (2H, d, J = 5.4 Hz, pic*H*), 6.83 (1H, d, J = 8.7 Hz, py*H*), 6.36 (1H, t, J = 6.4 Hz, py*H*), 2.31 (3H, s, C*H*$_3$). ^{13}C{^{1}H} NMR [CH_3CN-d_3, 125.7 MHz]: δ (ppm) 198.8 (C, *C*O) 198.7 (C, *C*O), 196.7 (C, *C*O), 153.0 (C, pic*C*$_{an}$), 152.1 (2C, pic*C*H$_{an}$), 149.8 (C, Ar*C*-NO$_2$), 149.2 (C, py*C*H), 142.5 (C, N═*C*H), 139.4 (C, Py*C*H), 137.4 (C, Ar*C*H), 136.3 (C, Ar*C*), 130.2 (C, Ar*C*H), 127.0 (2C, pic*C*H$_{an}$), 126.2 (C, Ar*C*H), 124.5 (C, Ar*C*H), 113.4 (C, py*C*H), 112.7 (C, py*C*H), 23.40 (C, *C*H$_3$). IR: ν (cm^{-1}) 2029 (*fac*-ν(C≡O)), 1909 (*fac*-ν(C≡O)), 1526 (ArNO$_2$, ν_{as}(N═O)$_2$), 1347 (ArNO$_2$, ν_{sym}(N═O)$_2$). HRMS (ESI$^+$) m/z calcd for $C_{15}H_{10}N_3O_3BrRe$: 547.9620. Found: 548.0091 {[M + H]$^+$, 100%}. RP-HPLC (System A): R_T (min) 14.1. Crystals suitable for X-ray crystallography were grown by slow evaporation the reaction mixture.

fac-[Re(CO)$_3$(HL^1)(pyridine)]BPh$_4$. This procedure is as that for *fac*-[Re(CO)$_3$(L^1)(4-picoline)], except using HL^1 (0.04 g, 0.15 mmol), *fac*-[Re(CO)$_3$(pyridine)$_3$]OTf (0.1 g, 0.15 mmol), and CH_3OH (4 mL). Analytical data refer to the deprotonated complex *fac*-[Re(CO)$_3$(L^1)(pyridine)] with no counterion present. ^{1}H NMR [CH_3CN-d_3, 500 MHz]: δ (ppm) 8.65 (2H, AA′XX′, Ar*H*), 8.50−8.49 (2H, m, py*H*$_{an}$), 8.35 (1H, ddd, J = 6.0, 1.7, 0.9 Hz, py*H*), 8.21 (2H, AA′XX′, Ar*H*), 7.89−7.86 (1H, m, py*H*$_{an}$), 7.88 (1H, s C*H*═N), 7.43 (1H, ddd, J = 8.7, 6.9, 1.8 Hz, py*H*), 7.36−7.33 (2H, m, py*H*$_{an}$), 6.90 (1H, dt, J = 8.7, 1.1 Hz, py*H*), 6.43 (1H, ddd, J = 6.9, 5.9, 1.2 Hz, py*H*). ^{13}C{^{1}H} NMR [CH_3CN-d_3, 125.7 MHz]: δ (ppm) 198.8 (C, *C*O), 198.7 (C, *C*O), 195.6 (C, *C*O), 170.3 (C, py*C*), 152.9 (2C, py*C*H$_{an}$), 149.1 (C, py*C*H), 141.5, 140.4, 139.2 (C, py*C*H$_{an}$), 132.1 (2C, Ar*C*H), 127.1 (2C, py*C*H$_{an}$), 124.2 (2C, Ar*C*H), 114.8 (2C, py*C*H), 113.2 (2C, py*C*H). IR: ν (cm^{-1}) 2034 (*fac*-ν(C≡O)), 1933 (*fac*-ν(C≡O)), 1902 (*fac*-ν(C≡O)), 1523 (ArNO$_2$, ν_{as}(N═O)$_2$). 1342 (ArNO$_2$, ν_{sym}(N═O)$_2$). HRMS (ESI$^+$) m/z calcd for $C_{20}H_{15}N_5O_5Re$: 592.0631. Found: 592.0692 {[M + H]$^+$, 100%}. RP-HPLC (System A): R_T (min) 13.4. Yellow block crystals suitable for X-ray crystallography were grown by the addition of excess $NaBPh_4$ to a concentrated solution of *fac*-[Re(CO)$_3$(L^1)(pyridine)] in CH_3OH followed by cooling at 0 °C for 3 days.

fac-[Re(CO)$_3$(L^2)(pyridine)]. This procedure is as that for *fac*-[Re(CO)$_3$(L^1)(4-picoline)], except using L^2 (0.04 g, 0.15 mmol), *fac*-[Re(CO)$_3$(pyridine)$_3$]OTf (0.1 g, 0.15 mmol), and CH_3OH (4 mL). Bright orange crystals were afforded as the desired product (1st crop) or orange powder (2nd crop; 0.06 g, 69%, total yield). ^{1}H NMR [CH_3CN-d_3, 500 MHz]: δ (ppm) 9.64 (1H, s, C*H*═N), 8.58 (1H, d, J = 7.9 Hz), 8.51 (2H, AA′XX′, py*H*), 8.33 (1H, dd, J = 5.9. 0.9 Hz, py*H*), 8.14 (1H, ddd, J = 8.2, 2.3, 0.9 Hz, py*H*), 7.92 (1H, s, py*H*), 7.88 (1H, tt, J = 7.7, 1.6 Hz, py*H*), 7.63 (1H, t, J = 8.0 Hz, py*H*), 7.41 (1H, ddd, J = 8.6, 6.9, 1.7 Hz), 7.37−7.34 (2H, AA′XX′, Ar*H*), 6.85 (1H, d, J = 8.7 Hz, py*H*). ^{13}C{^{1}H} NMR [CH_3CN-d_6, 125.7 MHz]: δ (ppm) 198.9 (2C, *C*O), 195.9 (C, *C*O), 153.0 (2C, py*C*H$_{an}$), 149.2 (C, Ar*C*-NO$_2$), 149.1 (C, Py*C*H), 142.1 (C, N═*C*H), 140.5 (C, py*C*H$_{an}$), 139.1 (C, Py*C*H), 137.5 (C, Ar*C*H), 136.3 (C, Ar*C*), 130.2 (C, Ar*C*H), 127.2 (2C, py*C*H$_{an}$), 126.2 (C, Ar*C*H), 123.9 (C, Ar*C*H), 114.4 (C, py*C*H), 112.7 (C, py*C*H). IR: ν (cm^{-1}) 2016 (*fac*-ν(C≡O)), 1893 (*fac*-ν(C≡O)), 1524 (ArNO$_2$, ν_{as}(N═O)$_2$), 1351 (ArNO$_2$, ν_{sym}(N═O)$_2$). HRMS (ESI$^+$) m/z calcd for $C_{20}H_{15}N_5O_5Re$ 592.0631. Found: 592.0635 {[M + H]$^+$, 100%}. RP-HPLC (System A): R_T (min) 13.5. Crystals suitable for X-ray crystallography were grown from a concentrated solution of methanol.

fac-[Re(CO)$_3$(L^1)(N,N′-dimethylaminopropylamine)]. This procedure is as that for *fac*-[Re(CO)$_3$(L^1)(4-picoline)], except using L^1 (0.03 g, 0.12 mmol) in hot CH_3OH (1 mL) and *fac*-[Re(CO)$_3$(DMAPA)$_3$]$^{2+}$ (approximately 0.12 mmol) in a 1:1 CH_3OH/DMAPA solution. Kugelrohr distillation was used to remove excess DMAPA. Dark red powder was obtained to afford the desired product (0.04 g, 55%). ^{1}H NMR [DMSO-d_6, 500 MHz]: δ (ppm) 8.69 (2H, AA′XX′, J = 9.5 Hz, Ar*H*), 8.24 (2H, AA′XX′, J = 9.0 Hz Ar*H*), 8.16 (1H, dd, J = 6.0, 0.5 Hz, py*H*), 7.66 (1H, s, N═C*H*), 7.52 (1H, t, J = 6.5 Hz, 1.6 Hz, py*H*), 7.00 (1H, d, J = 8.5 Hz, py*H*), 6.44 (1H, t, J = 6.5 Hz, py*H*), 4.13−4.04 (2H, m, NH$_2$C*H*$_2$CH$_2$CH$_2$N(CH$_3$)$_2$), 2.60−2.53 (2H, m, NH$_2$CH$_2$CH$_2$C*H*$_2$N(CH$_3$)$_2$), 2.11 (2H, m, NH$_2$C*H*$_2$CH$_2$CH$_2$N(CH$_3$)$_2$), 1.95 (6H, s, N(C*H*$_3$)$_2$), 1.47 (2H, quintet, J = 6.5 Hz, NH$_2$CH$_2$C*H*$_2$CH$_2$N(CH$_3$)$_2$). ^{13}C{^{1}H} NMR [DMSO-d_6, 125.7 MHz]: δ (ppm) 198.3 (2C, *C*O), 194.5 (C, *C*O), 168.9 (C, py*C*), 148.4 (C, ArNO$_2$), 145.3 (C, N═*C*H), 139.8 (py*C*H), 139.3 (C, py*C*H), 138.1 (C, Ar*C*), 130.9 (2C, Ar*C*H), 123.4 (2C, Ar*C*H), 113.9 (C, py*C*H), 111.9 (C, py*C*H), 57.6 (C, NH$_2$CH$_2$CH$_2$CH$_2$N(CH$_3$)$_2$), 47.3 (C, NH$_2$CH$_2$CH$_2$CH$_2$N(CH$_3$)$_2$), 44.8 (2C, N(CH$_3$)$_2$), 27.9 (C, NH$_2$CH$_2$CH$_2$CH$_2$N(CH$_3$)$_2$). IR: ν (cm^{-1}) 2007 (*fac*-ν(C≡O)), 1885 (*fac*-ν(C≡O)), 1874 (*fac*-ν(C≡O)), 1460 (ArNO$_2$, ν_{as}(N═O)$_2$), 1319 (ArNO$_2$, ν_{sym}(N═O)$_2$). ESI-MS m/z calcd for $C_{20}H_{24}N_6O_5Re$: 615.1366. Found: 615.1356 {[M + H]$^+$, 100%}. RP-HPLC (System A): R_T (min) 10.7.

L^5. To a solution of 1-(3-bromopropyl)-2-nitro-1*H*-imidazole[37] (0.10 g, 0.43 mmol; **1**) and di(2-picolyl)amine (0.08 mL, 0.43 mmol) in anhydrous THF (3 mL) was added *N*,*N*-DIPEA (0.07 mL, 0.39

DOI: 10.1021/acs.inorgchem.5b01691
Inorg. Chem. XXXX, XXX, XXX−XXX

mmol). The mixture was heated at reflux for 2 h then cooled to RT. The solution was reduced *in vacuo* and purified by column chromatography (EtOAc/CH_3OH, 60:40) to afford the desired compound in a moderate yield as yellow-orange oil (0.08 g, 55%). ^{1}H NMR [DMSO-d_6, 500 MHz]: δ (ppm) 8.48 (2H, d, J = 4.0 Hz, py*H*), 7.76 (2H, td, J = 7.6, 1.8 Hz, py*H*), 7.54 (1H, d, J = 1.0 Hz, ImC*H*), 7.49 (2H, d, J = 7.8 Hz, py*H*), 7.25 (2H, ddd, J = 7.4, 4.9, 1.1 Hz, py*H*), 7.10 (1H, d, J = 1.0 Hz, ImC*H*), 4.38 (2H, t, J = 7.3 Hz, CH_2), 3.74 (4H, s, CH_2), 2.02 (2H, quin, J = 7.2 Hz, CH_2), 1.25 (2H, m, CH_2). ^{13}C{^{1}H} NMR [CH_3CN-d_6, 125.7 MHz]: δ (ppm) 158.9 (2C, pyC), 148.7 (2C, pyCH), 136.4 (2C, pyCH), 127.7 (C, *C*H), 127.6 (C, *C*H), 122.8 (2C, pyCH), 122.1 (2C, pyCH), 59.4 (2C, CH_2), 50.1 (C, CH_2), 47.6 (C, CH_2), 27.2 (C, CH_2). IR: ν (cm^{-1}) 1400 (ImNO$_2$, ν_{as}(N═O)$_2$), 1321 (ImNO$_2$, ν_{sym}(N═O)$_2$). HRMS (ESI$^+$) m/z calcd for $C_{18}H_{21}N_6O_2$: 353.1726. Found: 353.1723 {[M + H]$^+$, 100%}. RP-HPLC (System A): R_T (min) 7.24.

*fac-[Re(CO)$_3$(**L**^{5})]BPh$_4$.* A degassed solution containing [Re(H$_2$O)$_5$(OTf)] (0.09 g, 0.19 mmol) and 3-(2-nitro-1*H*-imidazol-1-yl)-*N*,*N*-bis(2-pyridylmethyl)-1-propanamine (**L**^{5}; 0.07 g, 0.19 mmol) in methanol (5 mL) was subjected to microwave irradiation for 15 min at 120 °C. The solution was reduced *in vacuo*, and a concentrated solution of sodium tetraphenylborate (0.5 g, 1.4 mmol) in CH_3OH (1 mL) was added. An off-white solid precipitated out of solution and was collected via vacuum filtration (0.13 g, 73%). Crystals of X-ray crystallographic quality were grown via slow evaporation of the solid dissolved in acetonitrile. ^{1}H NMR [CH_3CN-d_3, 500 MHz]: δ (ppm) 8.75 (2H, s, py*H*), 7.84 (2H, td, J = 7.8, 1.5 Hz, py*H*), 7.39−7.36 (3H, m, C*H*), 7.27 (8H, m, BPh$_4$), 7.16 (1H, d, J = 1.0 Hz, C*H*), 6.99 (8H, t, J = 7.8 Hz, BPh$_4$), 6.84 (4H, t, J = 7.2 Hz, BPh$_4$), 4.60 (4H, s, CH_2), 4.51 (2H, t, J = 7.0 Hz, CH_2), 3.86−3.83 (2H, m, CH_2), 2.41−2.40 (2H, m, CH_2). ^{13}C{^{1}H} NMR [CH_3CN-d_6, 125.7 MHz]: δ (ppm) 196.9 (C, CO), 196.8 (2C, CO), 165.4 (C, BPh$_4$), 165.0 (C, BPh$_4$), 164.6 (C, BPh$_4$), 164.2 (C, BPh$_4$), 161.1 (C, pyC), 153.1 (2C, pyCH), 141.4 (2C, pyCH), 136.7 (8C, BPh$_4$), 129.2 (C, *C*H), 128.1 (C, *C*H), 126.7 (2C, pyCH), 126.6−126.5 (8C, BPh$_4$), 124.5 (2C, pyCH), 122.8 (4C, BPh$_4$), 68.4 (2C, CH_2), 67.8 (C, CH_2), 47.9 (C, CH_2), 26.7 (C, CH_2). IR: ν (cm^{-1}) 2027 (*fac*-ν(C≡O)), 1924 (*fac*-ν(C≡O)),1909 (*fac*-ν(C≡O)), 1482 (ImNO$_2$, ν_{as}(N═O)$_2$), 1365 (ImNO$_2$, ν_{sym}(N═O)$_2$). HRMS (ESI$^+$) m/z calcd for $C_{20}H_{15}N_5O_5Re$: 623.1053. Found: 623.1040 {[M]$^+$, 100%}. RP-HPLC (System A): R_T (min) 4.97

***L*^{6}*Et*.** Ethyl *N*-(2-pyridylmethyl)amino acetate (0.09 g, 0.43 mmol; **2**) was added to a solution of 1-(3-bromopropyl)-2-nitro-1*H*-imidazole (0.10 g, 0.43 mmol; **1**) in dry CH_3CN (7 mL) and *N*,*N*-DIPEA (0.10 mL, 0.6 mmol). The reaction was heated to reflux overnight, then cooled and concentrated *in vacuo*. Purification by column chromatography (EtOAc/hexane, 96:4) afforded clear oil (0.03 g, 21%). ^{1}H NMR [$CHCl_3$-*d*, 500 MHz]: δ (ppm) 8.87 (1H, ddd, J = 5.6, 1.6, 0.7 Hz, py*H*), 8.26 (1H, td, J = 7.8, 1.7 Hz, py*H*), 7.92 (1H, dd, J = 8.0, 0.5 Hz, py*H*), 7.73 (1H, ddd, J = 7.6, 5.7, 1.3 Hz, py*H*), 7.22 (1H, d, J = 1.1 Hz, ImC*H*), 7.12 (1H, d, J = 1.1 Hz, ImC*H*), 4.49−4.46 (2H, m, CH_2), 4.32 (2H, s, CH_2), 4.19 (2H, q, J = 7.2 Hz, CH_2), 3.54 (2H, s, CH_2), 2.90 (2H, t, J = 6.8 Hz, CH_2), 2.06 (2H, quin, J = 7.3 Hz, CH_2), 1.27 (3H, t, J = 7.2 Hz, CH_2). ^{13}C{^{1}H} NMR [$CHCl_3$-*d*, 125.7 MHz]: δ (ppm) 170.2 (C, CO_2Et), 155.2 (C, pyC), 144.0 (C, pyCH), 143.7 (C, pyCH), 128.6 (C, *C*H), 126.6 (C, *C*H), 126.3 (C, pyCH), 125.3 (C, pyCH), 61.4 (C, CH_2), 56.0 (C, CH_2), 54.4 (C, CH_2), 51.4 (C, CH_2), 48.0 (C, CH_2), 28.3 (C, CH_2), 14.3 (C, CH_3). IR: ν (cm^{-1}) 1730 (m/sh, C═O), 1555 (ν_{as}(N═O)$_2$), 1340 (ν_{sym}(N═O)$_2$). HRMS (ESI$^+$) m/z calcd for $C_{16}H_{22}N_5O_4$: 348.1672. Found: 348.1874 {[M + H]$^+$, 100%}. RP-HPLC (System B): R_T (min) 11.2.

*fac-[Re(CO)$_3$(**L**^{6})].* Sodium hydroxide (3.45 mg, 0.09 mmol) and **L**^{6}Et (0.03 g, 0.09 mmol) in CH_3CN (4 mL) were heated at reflux for 2 h. The solvent was reduced *in vacuo* and a solution of [Re(CO)$_5$OTf] (0.04 g, 0.09 mmol) in CH_3OH (4 mL) added and subjected to microwave irradiation for 15 min at 120 °C. The solvent was concentrated to 1 mL and Et_2O added. The precipitate was collected via vacuum filtration and washed with copious amounts of cold Et_2O to afford an off-white solid (0.03 g, 60%). ^{1}H NMR [DMSO-d_6, 500 MHz]: δ (ppm) 8.75 (1H, d, J = 4.5, Hz, py*H*), 8.14 (1H, t, J = 7.5 Hz, py*H*), 7.69 (1H, s, ImC*H*), 7.67 (1H, d, py*H*), 7.57 (1H, t, J = 6.0 Hz, pyC*H*), 7.23 (1H, s, ImC*H*), 4.77 (1H, d, $^2J_{HH}$ = 16 Hz, NCH_2CO$_2$), 4.51 (1H, obscd d, NCH_2CO$_2$), 4.49 (2H, br t, NCH$_2$CH$_2$CH_2Im), 3.82 (1H, d, $^2J_{HH}$ = 17 Hz, NCH_2Py), 3.62−3.54 (2H, m, NCH_2CH$_2$CH$_2$Im), 3.38 (1H, obsc'd d, NCH_2Py), 2.39−2.28 (2H, m, NCH$_2$CH_2CH$_2$Im). ^{13}C{^{1}H} NMR [DMSO-d_6, 125.7 MHz]: δ (ppm) 198.9 (C, CO), 196.5 (2C, CO), 185.6 (C, CO_2), 161.0 (C, pyC), 150.1 (C, pyCH), 146.4 (C, pyCH), 135.9 (C, ImCH), 130.1 (C, ImCH), 128.6 (C, pyCH), 127.6 (C, pyCH), 62.8 (C, CH_2), 62.4 (C, CH_2), 56.8 (C, CH_2), 49.9 (C, CH_2), 29.2 (C, CH_2). IR: ν (cm^{-1}) 2012 (*fac*-ν(C≡O)), 1900 (*fac*-ν(C≡O)), 1874 (*fac*-ν(C≡O)), 1652 (ν_{as}(C ¨ O)$_2$), 1485 (ν_{as}(N═O)$_2$), 1365 (ν_{sym}(C ¨ O)$_2$), 1339 (ν_{sym}(N═O)$_2$). ESI-MS m/z calcd for $C_{17}H_{17}N_5O_7Re$ 590.0686. Found: 590.0700 {[M + H]$^+$, 100%}. RP-HPLC (System A): R_T (min) 10.8.

*fac-[^{99m}Tc(CO)$_3$(**L**$^{5/6}$)].* Technetium-99m labeling of **L**^{5} and H**L**^{6} involved the initial synthesis of technetium tricarbonyl precursor, *fac*-[^{99m}Tc(H$_2$O)$_3$(CO)$_3$]$^+$. Sodium pertechnetate, Na[^{99m}TcO$_4$], was eluted from a Gentech ^{99} Mo/^{99m}Tc sterile generator (1000 MBq, Austin Health, Heidelberg, Australia, via ANSTO Health) as a 1.0 mL saline solution (0.9% v/v). The radioactive solution was then added to an evacuated Isolink vial (Mallinckrodt Pharmaceuticals, The Netherlands) and heated for 20 min at 100 °C. The solution was cooled to room temperature. Separate solutions of ligands **L**^{5} and **L**^{6}Et in acetonitrile/water (1:2 v/v) were prepared (6.7 mg mL^{-1}). To the aqueous *fac*-[^{99m}Tc(H$_2$O)$_3$(CO)$_3$]$^+$ solution (0.1 mL) was added 0.1 M HCl, (~25 μL), 0.1 M PBS buffer (50 μL pH 7.4), and the ligand stock solution (20 μL). The pH was adjusted to 7−8 with additional 0.1 M HCl if required. The mixtures were heated to 65 °C for 30 min. Aliquots (20 μL) of the reaction mixture were injected onto the analytical RP-HPLC column (Column 7, System C) for UV and radioactivity analysis.

*Partition Coefficient and Stability Measurements for Radiolabeled Complex fac-[^{99m}Tc(CO)$_3$(**L**^{5})]$^+$.* Partition coefficients were determined by the addition of *fac*-[^{99m}Tc(CO)$_3$(**L**^{5})]$^+$ (10 μL, ~ 5 MBq without decay correction) to an octanol/0.1 M PBS (pH 7.4) solution (1:1 v/v). The mixture was shaken for 3 min; then the layers were left to separate. An aliquot of the organic layer (0.9 mL octanol) was added to freshly prepared 0.1 M PBS (0.9 mL), and each phase was presaturated with the other phase and shaken for 3 min. The mixture was centrifuged (5 min, 13 200 rpm) and aliquots (0.5 mL) from the two separate layers (aqueous and organic) taken for analysis of the radioactive decay. All samples were prepared and measured in triplicate.

For serum stability studies, 20 mL of blood from a healthy male was centrifuged (10 min, 3000 rpm) to separate blood plasma and red blood cells. The plasma was transferred to a separate vial and the red blood cells discarded. An aliquot of plasma (0.6 mL) was added to labeled compound *fac*-[^{99m}Tc(CO)$_3$(**L**^{5})]$^+$ (0.15 mL), the radioactivity monitored, and the mixture then incubated at 37 °C. Aliquots (0.1 mL) of the mixture were removed from heating at 10 min and every 2 h following (over 6 h), and acetonitrile (0.1 mL) was added to the serum/tracer mix to precipitate serum proteins. The suspension was shaken for 5 min, then centrifuged (5 min, 13 200 rpm). The radioactivity of the supernatant and pellet was recorded. The supernatant (20 μL) was analyzed by analytical RP-HPLC (System C) for UV and radioactivity analysis and the pellet washed with acetonitrile (3 × 0.1 mL), and the radioactivity levels were again recorded (radioactivity levels of the pellet were negligible).

Confocal Fluorescent Microscopy. Human carcinoma HeLa cells were grown on poly-L-lysine (PLL) coated coverslips and incubated at 37 °C (95% air, 5% CO_2). When cells had reached approximately 80% confluency, they were treated with 5, 10, 25, and 50 μM solutions of *fac*-[Re(CO)$_3$(**L**$^{1-2}$)(4-picoline)] in DMSO, λ_{ex} = 520 nm. Cell treatments were for 30 min. Cells were then rinsed with 1% PBS and fixed with 4% (w/v) paraformaldehyde for 20 min at ambient temperature. Following fixation, cells were rinsed twice with 1% PBS and mounted onto glass slides using DAKO fluorescence mounting medium, and images were collected. Images of the cells were collected using an Olympus FV1000 IV81 confocal microscope.

DOI: 10.1021/acs.inorgchem.5b01691
Inorg. Chem. XXXX, XXX, XXX−XXX

Cellular Assays. Cell uptake studies were carried out with the assistance of Dr. Christine Schieber and Ms. Irene Volitakis. Compounds were prepared as 10 mM stock solutions in culture-grade DMSO, and the control compound $[Re(CO)_5OTf]$ was prepared as a 10 mM stock solution in Milli-Q water. To each complex sample (50 μL) was added warmed, serum-free media (DMEM/F12 + P/S + NEAA + HEPES, 50 mL) for a final media solution concentration of 10 μM.

SH-(SY5Y) cells were grown continuously and passaged at regular intervals. Cells were removed from the tissue culture flask once 90% confluent and then grown in Petri dishes until approximately 60% confluency had been reached. Half the Petri dishes were placed in a BD GasPak EZ gas generating chamber with two activated gas-generating sachets (BD GasPak EZ ref: 260001, Anaerobe Container System with Indicator) for 16 h. Low oxygen was confirmed for each assay as per the manufacturer's instructions.

For nonhypoxic (normoxic) cells, media were aspirated off the cells that were not in the anaerobic chamber and replaced with 10 mL of the media/complex solution (per plate in quadruplets). The cells were then incubated for 60 min at 37 °C; DMSO was used as a vehicle control whereby cells were treated and incubated under the same conditions. For oxygen-depleted (hypoxic) cells, Petri dishes were removed from the anaerobic container system, and the existing media were replaced with fresh media solutions, which had been deoxygenated with N_2 gas over 10 min. Freshly prepared treatment solution (10 μM media/complex) was also degassed and then added to the cells after removal of the media. Cells were again placed in the GasPak EZ container with three new GasPak bags and incubated for 60 min at 37 °C; DMSO was used as a vehicle control whereby cells were treated and incubated under the same conditions.

Cells were scraped into the media and transferred into 15 mL Eppendorf tubes, which were centrifuged for 3 min (1500 rpm). The supernatant was removed and the pellet washed with PBS (2 × 5 mL). The cell pellet was resuspended in 1 mL of PBS and 100 μL removed for a BCA protein assay. The remaining mixture was centrifuged for 3 min (1500 rpm) and the PBS supernatant discarded. Cell pellets were stored at −20 °C.

Rhenium levels were measured using a Varian UltraMass ICP-MS instrument and quoted relative to protein measured by bicinchoninic acid (BCA) protein assay. BCA protein assay was undertaken via a 10-fold dilution (with PBS) of the 100 μL cell-pellet/PBS mixture acquired earlier. A solution of BCA−reagent mixture, consisting of reagent A and reagent B (50:1), was prepared. Working solutions and standards (25 μL) were pipetted into 96-well microplates, followed by the addition of BCA−reagent (200 μL per well). The plates were covered in foil and incubated at 25 °C for 30 min, and the absorbance was read at λ 562 nm for the colorimetric detection and quantitation of total protein in the cells.

Animal SPECT Imaging Studies with fac-$[^{99m}Tc(CO)_3(L^5)]^+$. All animal experiments were approved by the Austin Hospital animal ethics committee. SPECT/CT studies involved the same labeling procedure as covered above, except that half the amount of radioactivity was used (approximately 50 MBq) per sample. SK-RC-52 tumors were first grown by injecting suspensions of 6×10^6 of SK-RC-52 tumor cells in saline subcutaneously into the flank of the three BALB/c nude mice. Tumours were allowed to grow to a size of about 300 mm^3, then cut into 40 mm^3 pieces and transplanted into the shoulder of the BALB/c nude mice. Imaging was undertaken when the tumors were 400 mm^3 (Mouse 1), 600 mm^3 (Mouse 2), and 1100 mm^3 (Mouse 3) in size. A cannula was inserted into the lateral tail vein of Mouse 1, Mouse 2, and Mouse 3 and 21, 18, and 19 MBq of *fac*-$[^{99m}Tc(CO)_3(L^5)]^+$ respectively administered in 0.1 M PBS and 2% ethanol. Animals were anaesthetized with 5.0% isoflurane in air for induction and 2.5% isoflurane in air while the animal was on the scanning bed, with a Minerva Biovet animal imaging system. The Minerva Biovet system also provided a temperature-stabilized environment for the animals during the induction and imaging stages and respiration rate was monitored. A 10 min static frame was acquired for all three mice 2 h post injection. Images were reconstructed using a pinhole MLEM algorithm. FMISO was produced at Austin Health following a previously reported procedure.[57]

■ ASSOCIATED CONTENT

Supporting Information

The Supporting Information is available free of charge on the ACS Publications website at DOI: 10.1021/acs.inorgchem.5b01691.

Summary of crystal data and structure refinement for *fac*-$[Re(CO)_3(HL^3)(Br)]$ and *fac*-$[Re(CO)_3(HL^4)(Br)]$ is also given (PDF)

Crystallographic Information Files (CIF) for compounds: HL^1, HL^2, *fac*-$[Re(CO)_3(HL^1)Br]$, *fac*-$[Re(CO)_3(H^L2)Br]$, *fac*-$[Re(CO)_3(HL^3)Br]$, *fac*-$[Re(CO)_3(HL^4)Br]$, *fac*-$[Re(CO)_3(HL^1)(pyridine)]BPh_4$, *fac*-$[Re(CO)_3(L^1)(4\text{-picoline})]$, *fac*-$[Re(CO)_3(L^2)(pyridine)]$, *fac*-$[Re(CO)_3(L^2)(4\text{-picoline})]$, and *fac*-$[Re(CO)_3(L^5)]BPh_4$. Cambridge Crystallographic Data Centre numbers 1416475-1416485. Crystallographic Information File (CIF)

Crystallographic Information File (CIF)

Crystallographic Information File (CIF)

Crystallographic Information File (CIF)

Crystallographic Information File (CIF)

Crystallographic Information File (CIF)

Crystallographic Information File (CIF)

Crystallographic Information File (CIF)

Crystallographic Information File (CIF)

Crystallographic Information File (CIF)

■ AUTHOR INFORMATION

Corresponding Author

*E-mail: pauld@unimelb.edu.au.

Author Contributions

The manuscript was written through contributions of all authors. All authors have given approval to the final version of the manuscript.

Notes

The authors declare no competing financial interest.

■ ACKNOWLEDGMENTS

The Australian Research Council and the National Health and Medical Research Council are thanked for partial funding of this research. The imaging equipment used for the animal nanoSPECT/CT studies was purchased by the Australian Cancer Research Foundation's Centre for Translational Cancer Therapeutics. P.S.D. is an ARC Future Fellow. A.J.N. acknowledges the Albert Shimmins' Postgraduate Writing-Up Award.

■ REFERENCES

(1) Chia, K.; Fleming, I. N.; Blower, P. J. *Nucl. Med. Commun.* **2012**, *33*, 217−22.

(2) Jerabek, P. A.; Patrick, T. B.; Kilbourn, M. R.; Dischino, D. D.; Welch, M. J. *Appl. Radiat. Isot.* **1986**, *37*, 599−605.

(3) Lee, S.; Scott, A. *Semin. Nucl. Med.* **2007**, *37*, 451−461.

(4) Zimny, M.; Gagel, B.; Dimartino, E.; Hamacher, K.; Coenen, H. H.; Westhofen, M.; Eble, M.; Buell, U.; Reinartz, P. *Eur. J. Nucl. Med. Mol. Imaging* **2006**, *33*, 1426−31.

(5) Nunn, A.; Linder, K.; Strauss, H. W. *Eur. J. Nucl. Med.* **1995**, *22*, 265−80.

DOI: 10.1021/acs.inorgchem.5b01691
Inorg. Chem. XXXX, XXX, XXX−XXX

(6) Ricardo, C. L.; Kumar, P.; Wiebe, L. I. *J. Diagn. Imaging Ther.* **2015**, *2*, 103−58.
(7) Linder, K. E.; Chan, Y. W.; Cyr, J. E.; Malley, M. F.; Nowotnik, D. P.; Nunn, A. D. *J. Med. Chem.* **1994**, *37*, 9−17.
(8) Melo, T.; Tunggal, J. K.; Ballinger, J. R.; Rauth, A. M. *Cancer Biother.Radiopharm.* **2002**, *17*, 515−26.
(9) Melo, T.; Duncan, J.; Ballinger, J. R.; Rauth, A. M. *J. Nucl. Med.* **2000**, *41*, 169−176.
(10) Zhang, X.; Melo, T.; Ballinger, J. R.; Rauth, A. M. *Int. J. Radiat. Oncol., Biol., Phys.* **1998**, *42*, 737−40.
(11) Zhang, X.; Melo, T.; Rauth, A. M.; Ballinger, J. R. *Nucl. Med. Biol.* **2001**, *28*, 949−57.
(12) Su, Z.-F.; Ballinger, J.; Rauth, A.; Abrams, D.; Billinghurst, M. *Bioconjugate Chem.* **2000**, *11*, 652−63.
(13) Zhang, X.; Su, Z. F.; Ballinger, J. R.; Rauth, A. M.; Pollak, A.; Thornback, J. R. *Bioconjugate Chem.* **2000**, *11*, 401−7.
(14) Su, Z.-F.; Zhang, X.; Ballinger, J.; Rauth, A.; Pollak, A.; Thornback, J. *Bioconjugate Chem.* **1999**, *10*, 897−904.
(15) Denny, W. A. *Lancet Oncol.* **2000**, *1*, 25−9.
(16) Tercel, M.; Wilson, W. R.; Anderson, R. F.; Denny, W. A. *J. Med. Chem.* **1996**, *39*, 1084−94.
(17) Tercel, M.; Lee, A. E.; Hogg, A.; Anderson, R. F.; Lee, H. H.; Siim, B. G.; Denny, W. A.; Wilson, W. R. *J. Med. Chem.* **2001**, *44*, 3511−22.
(18) Alberto, R.; Schibli, R.; Waibel, R.; Abram, U.; Schubiger, A. P. *Coord. Chem. Rev.* **1999**, *190−192*, 901−19.
(19) Liu, S. *Adv. Drug Delivery Rev.* **2008**, *60*, 1347−70.
(20) Banerjee, S. R.; Levadala, M. K.; Lazarova, N.; Wei, L.; Valliant, J. F.; Stephenson, K. A.; Babich, J. W.; Maresca, K. P.; Zubieta, J. *Inorg. Chem.* **2002**, *41*, 6417−25.
(21) Ganguly, T.; Kasten, B. B.; Bučar, D.-K.; Macgillivray, L. R.; Berkman, C. E.; Benny, P. D. *Chem. Commun.* **2011**, *47*, 12846−8.
(22) Bartholomä, M.; Valliant, J.; Maresca, K. P.; Babich, J.; Zubieta, J. *Chem. Commun.* **2009**, 493−512.
(23) Wang, J.; Zheng, X.; Wu, W.; Yang, W.; liu, Y. *J. Radioanal. Nucl. Chem.* **2014**, *300*, 1013−20.
(24) Sagnou, M.; Tzanopoulou, S.; Raptopoulou, C. P.; Psycharis, V.; Braband, H.; Alberto, R.; Pirmettis, I. C.; Papadopoulos, M.; Pelecanou, M. *Eur. J. Inorg. Chem.* **2012**, *27*, 4279−4286.
(25) Giglio, J.; Patsis, G.; Pirmettis, I.; Papadopoulos, M.; Raptopoulou, C.; Pelecanou, M.; Leon, E.; Gonzalez, M.; Cerecetto, H.; Rey, A. *Eur. J. Med. Chem.* **2008**, *43*, 741−8.
(26) Mallia, M. B.; Kumar, C.; Mathur, A.; Sarma, H. D.; Banerjee, S. *Nucl. Med. Biol.* **2012**, *39*, 1236−42.
(27) Mallia, M. B.; Subramanian, S.; Mathur, A.; Sarma, H. D.; Venkatesh, M.; Banerjee, S. *J. Labelled Compd. Radiopharm.* **2010**, *53*, 535−42.
(28) Mallia, M. B.; Subramanian, S.; Mathur, A.; Sarma, H. D.; Banerjee, S. *Nucl. Med. Biol.* **2014**, *41*, 600−10.
(29) Mallia, M. B.; Mathur, A.; Sarma, H. D.; Banerjee, S. *Cancer Biother.Radiopharm.* **2015**, *30*, 79−86.
(30) Wrighton, M. S.; Morse, D. L. *J. Am. Chem. Soc.* **1974**, *96*, 998−1003.
(31) Connelly, N. G.; Geiger, W. E. *Chem. Rev.* **1996**, *96*, 877−910.
(32) Squella, J. A.; Campero, A.; Maraver, J.; Carbajo, J. *Electrochim. Acta* **2006**, *52*, 511−8.
(33) Roffia, S.; Gottardi, C. *J. Electroanal. Chem. Interfacial Electrochem.* **1982**, *142*, 263−275.
(34) Linder, K. E.; Chan, Y. W.; Cyr, J. E.; Nowotnik, D. P.; Eckelman, W. C.; Nunn, A. D. *Bioconjugate Chem.* **1993**, *4*, 326−33.
(35) Moya, S. A.; Guerrero, J.; Pastene, R.; Schmidt, R.; Sariego, R. *Inorg. Chem.* **1994**, *33*, 2341−2346.
(36) Agrawal, K. C.; Bears, K. B.; Sehgal, R. K.; Brown, J. N.; Rist, P. E.; Rupp, W. D. *J. Med. Chem.* **1979**, *22*, 583−6.
(37) Long, A.; Parrick, J.; Hodgkiss, R. J. *Synthesis* **1991**, *9*, 709−713.
(38) Silverstein, R. M.; Webster, F. X.; Kiemle, D. *Spectrometric Identification of Organic Compounds*, 7th ed.; John Wiley & Sons, Inc.: New York, 2005.
(39) Chiotellis, A.; Tsoukalas, C.; Pelecanou, M.; Raptopoulou, C.; Terzis, A.; Papadopoulos, M.; Papadopoulou-Daifoti, Z.; Pirmettis, I. *Inorg. Chem.* **2008**, *47*, 2601−7.
(40) Frantz, S.; Fiedler, J.; Hartenbach, I.; Schleid, T.; Kaim, W. *J. Organomet. Chem.* **2004**, *689*, 3031−9.
(41) Lo, K. K.-W.; Zhang, K. Y.; Li, S. P.-Y. *Eur. J. Inorg. Chem.* **2011**, *2011*, 3551−68.
(42) Thorp-Greenwood, F. L.; Coogan, M. P. *Dalton Trans.* **2011**, *40*, 6129−43.
(43) Balasingham, R. G.; Coogan, M. P.; Thorp-Greenwood, F. L. *Dalton Trans.* **2011**, *40*, 11663−74.
(44) Fernandez-Moreira, V.; Thorp-Greenwood, F. L.; Amoroso, A. J.; Cable, J.; Court, J. B.; Gray, V.; Hayes, A. J.; Jenkins, R. L.; Kariuki, B. M.; Lloyd, D.; Millet, C. O.; Williams, C. F.; Coogan, M. P. *Org. Biomol. Chem.* **2010**, *8*, 3888−901.
(45) Fernandez-Moreira, V.; Thorp-Greenwood, F. L.; Coogan, M. P. *Chem. Commun.* **2010**, *46*, 186−202.
(46) Fuks, L.; Gniazdowska, E.; Kozminski, P.; Lyczko, M.; Mieczkowski, J.; Narbutt, J. *Appl. Radiat. Isot.* **2010**, *68*, 90−5.
(47) Lawrentschuk, N.; Poon, A. M. T.; Foo, S. S.; Putra, L. G. J.; Murone, C.; Davis, I. D.; Bolton, D. M.; Scott, A. M. *BJU Int.* **2005**, *96*, 540−6.
(48) Höckel, M.; Schlenger, K.; Aral, B.; Mitze, M.; Schäffer, U.; Vaupel, P. *Cancer. Res.* **1996**, *56*, 4509−15.
(49) Lawrentschuk, N.; Lee, F.; Jones, G.; Rigopoulos, A.; Mountain, A.; O'Keefe, G.; Papenfuss, A. T.; Bolton, D.; Davis, I.; Scott, A. M. *Urol.Oncol.* **2011**, *29*, 411−420.
(50) Schmidt, S. P.; Nitschke, J.; Trogler, W. C. *Inorg. Synth.* **1989**, *26*, 113−7.
(51) Weinmann, H.; Harre, M.; Koenig, K.; Merten, E.; Tilstam, U. *Tetrahedron Lett.* **2002**, *43*, 593−5.
(52) Tzanopoulou, S.; Pirmettis, I. C.; Patsis, G.; Paravatou-Petsotas, M.; Livaniou, E.; Papadopoulos, M.; Pelecanou, M. *J. Med. Chem.* **2006**, *49*, 5408−10.
(53) Todeschini, A. R.; de Miranda, A. L. P.; da Silva, K. C. M.; Parrini, S. C.; Barreiro, E. J. *Eur. J. Med. Chem.* **1998**, *33*, 189−99.
(54) Karabatsos, G. J.; Graham, J. D.; Vane, F. M. *J. Am. Chem. Soc.* **1962**, *84*, 753−55.
(55) Schutte, E. J.; Sullivan, P. B. *Inorg. Synth.* **2002**, *33*, 227−30.
(56) He, H.; Lipowska, M.; Xu, X.; Taylor, A. T.; Carlone, M.; Marzilli, L. G. *Inorg. Chem.* **2005**, *44*, 5437−46.
(57) Tochon-Danguy, H. J.; Sachinidis, J. I.; Chan, F.; Chan, J. G.; Hall, C.; Cher, L.; Stylli, S.; Hill, J.; Kaye, A.; Scott, A. M. *Nucl. Med. Biol.* **2002**, *29*, 191−7.

DOI: 10.1021/acs.inorgchem.5b01691
Inorg. Chem. XXXX, XXX, XXX−XXX